THE UNIVERSITY OF CALGARY

FREQUENCY RESPONSE PHASE ESTIMATION OF THE UHF INDOOR COMMUNICATIONS CHANNEL

BY

BRIAN PAUL DONALDSON

A THESIS

SUBMITTED TO THE FACULTY OF GRADUATE STUDIES

IN PARTIAL FULFILLMENT OF THE REQUIREMENTS FOR THE

DEGREE OF MASTER OF ENGINEERING

DEPARTMENT OF ELECTRICAL AND COMPUTER ENGINEERING

CALGARY, ALBERTA

MARCH, 1993

ISBN 0-315-83134-0

Name Brian Donaldson

Dissertation Abstracts International is arranged by broad, general subject categories. Please select the one subject which most nearly describes the content of your dissertation. Enter the corresponding four-digit code in the spaces provided.

Engineering - Electronics & Electrical | 0544 | U·M·I

SUBJECT TERM | SUBJECT CODE

Subject Categories

THE HUMANITIES AND SOCIAL SCIENCES

COMMUNICATIONS AND THE ARTS
Architecture 0729
Art History 0377
Cinema 0900
Dance 0378
Fine Arts 0357
Information Science 0723
Journalism 0391
Library Science 0399
Mass Communications 0708
Music 0413
Speech Communication 0459
Theater 0465

EDUCATION
General 0515
Administration 0514
Adult and Continuing 0516
Agricultural 0517
Art 0273
Bilingual and Multicultural 0282
Business 0688
Community College 0275
Curriculum and Instruction 0727
Early Childhood 0518
Elementary 0524
Finance 0277
Guidance and Counseling 0519
Health 0680
Higher 0745
History of 0520
Home Economics 0278
Industrial 0521
Language and Literature 0279
Mathematics 0280
Music 0522
Philosophy of 0998
Physical 0523
Psychology 0525
Reading 0535
Religious 0527
Sciences 0714
Secondary 0533
Social Sciences 0534
Sociology of 0340
Special 0529
Teacher Training 0530
Technology 0710
Tests and Measurements 0288
Vocational 0747

LANGUAGE, LITERATURE AND LINGUISTICS
Language
- General 0679
- Ancient 0289
- Linguistics 0290
- Modern 0291

Literature
- General 0401
- Classical 0294
- Comparative 0295
- Medieval 0297
- Modern 0298
- African 0316
- American 0591
- Asian 0305
- Canadian (English) 0352
- Canadian (French) 0355
- English 0593
- Germanic 0311
- Latin American 0312
- Middle Eastern 0315
- Romance 0313
- Slavic and East European 0314

PHILOSOPHY, RELIGION AND THEOLOGY
Philosophy 0422
Religion
- General 0318
- Biblical Studies 0321
- Clergy 0319
- History of 0320
- Philosophy of 0322

Theology 0469

SOCIAL SCIENCES
American Studies 0323
Anthropology
- Archaeology 0324
- Cultural 0326
- Physical 0327

Business Administration
- General 0310
- Accounting 0272
- Banking 0770
- Management 0454
- Marketing 0338

Canadian Studies 0385
Economics
- General 0501
- Agricultural 0503
- Commerce-Business 0505
- Finance 0508
- History 0509
- Labor 0510
- Theory 0511

Folklore 0358
Geography 0366
Gerontology 0351
History
- General 0578
- Ancient 0579
- Medieval 0581
- Modern 0582
- Black 0328
- African 0331
- Asia, Australia and Oceania 0332
- Canadian 0334
- European 0335
- Latin American 0336
- Middle Eastern 0333
- United States 0337

History of Science 0585
Law 0398
Political Science
- General 0615
- International Law and Relations 0616
- Public Administration 0617

Recreation 0814
Social Work 0452
Sociology
- General 0626
- Criminology and Penology 0627
- Demography 0938
- Ethnic and Racial Studies 0631
- Individual and Family Studies 0628
- Industrial and Labor Relations 0629
- Public and Social Welfare 0630
- Social Structure and Development 0700
- Theory and Methods 0344

Transportation 0709
Urban and Regional Planning 0999
Women's Studies 0453

THE SCIENCES AND ENGINEERING

BIOLOGICAL SCIENCES
Agriculture
- General 0473
- Agronomy 0285
- Animal Culture and Nutrition 0475
- Animal Pathology 0476
- Food Science and Technology 0359
- Forestry and Wildlife 0478
- Plant Culture 0479
- Plant Pathology 0480
- Plant Physiology 0817
- Range Management 0777
- Wood Technology 0746

Biology
- General 0306
- Anatomy 0287
- Biostatistics 0308
- Botany 0309
- Cell 0379
- Ecology 0329
- Entomology 0353
- Genetics 0369
- Limnology 0793
- Microbiology 0410
- Molecular 0307
- Neuroscience 0317
- Oceanography 0416
- Physiology 0433
- Radiation 0821
- Veterinary Science 0778
- Zoology 0472

Biophysics
- General 0786
- Medical 0760

EARTH SCIENCES
Biogeochemistry 0425
Geochemistry 0996
Geodesy 0370
Geology 0372
Geophysics 0373
Hydrology 0388
Mineralogy 0411
Paleobotany 0345
Paleoecology 0426
Paleontology 0418
Paleozoology 0985
Palynology 0427
Physical Geography 0368
Physical Oceanography 0415

HEALTH AND ENVIRONMENTAL SCIENCES
Environmental Sciences 0768
Health Sciences
- General 0566
- Audiology 0300
- Chemotherapy 0992
- Dentistry 0567
- Education 0350
- Hospital Management 0769
- Human Development 0758
- Immunology 0982
- Medicine and Surgery 0564
- Mental Health 0347
- Nursing 0569
- Nutrition 0570
- Obstetrics and Gynecology 0380
- Occupational Health and Therapy 0354
- Ophthalmology 0381
- Pathology 0571
- Pharmacology 0419
- Pharmacy 0572
- Physical Therapy 0382
- Public Health 0573
- Radiology 0574
- Recreation 0575
- Speech Pathology 0460
- Toxicology 0383

Home Economics 0386

PHYSICAL SCIENCES

Pure Sciences
Chemistry
- General 0485
- Agricultural 0749
- Analytical 0486
- Biochemistry 0487
- Inorganic 0488
- Nuclear 0738
- Organic 0490
- Pharmaceutical 0491
- Physical 0494
- Polymer 0495
- Radiation 0754

Mathematics 0405
Physics
- General 0605
- Acoustics 0986
- Astronomy and Astrophysics 0606
- Atmospheric Science 0608
- Atomic 0748
- Electronics and Electricity 0607
- Elementary Particles and High Energy 0798
- Fluid and Plasma 0759
- Molecular 0609
- Nuclear 0610
- Optics 0752
- Radiation 0756
- Solid State 0611

Statistics 0463

Applied Sciences
Applied Mechanics 0346
Computer Science 0984
Engineering
- General 0537
- Aerospace 0538
- Agricultural 0539
- Automotive 0540
- Biomedical 0541
- Chemical 0542
- Civil 0543
- Electronics and Electrical 0544
- Heat and Thermodynamics 0348
- Hydraulic 0545
- Industrial 0546
- Marine 0547
- Materials Science 0794
- Mechanical 0548
- Metallurgy 0743
- Mining 0551
- Nuclear 0552
- Packaging 0549
- Petroleum 0765
- Sanitary and Municipal 0554
- System Science 0790

Geotechnology 0428
Operations Research 0796
Plastics Technology 0795
Textile Technology 0994

PSYCHOLOGY
General 0621
Behavioral 0384
Clinical 0622
Developmental 0620
Experimental 0623
Industrial 0624
Personality 0625
Physiological 0989
Psychobiology 0349
Psychometrics 0632
Social 0451

Nom ____________________

Dissertation Abstracts International est organisé en catégories de sujets. Veuillez s.v.p. choisir le sujet qui décrit le mieux votre thèse et inscrivez le code numérique approprié dans l'espace réservé ci-dessous.

____________________ SUJET | ☐☐☐☐ CODE DE SUJET | U·M·I

Catégories par sujets

HUMANITÉS ET SCIENCES SOCIALES

COMMUNICATIONS ET LES ARTS
Architecture 0729
Beaux-arts 0357
Bibliothéconomie 0399
Cinéma 0900
Communication verbale 0459
Communications 0708
Danse 0378
Histoire de l'art 0377
Journalisme 0391
Musique 0413
Sciences de l'information 0723
Théâtre 0465

ÉDUCATION
Généralités 515
Administration 0514
Art 0273
Collèges communautaires 0275
Commerce 0688
Économie domestique 0278
Éducation permanente 0516
Éducation préscolaire 0518
Éducation sanitaire 0680
Enseignement agricole 0517
Enseignement bilingue et multiculturel 0282
Enseignement industriel 0521
Enseignement primaire. 0524
Enseignement professionnel 0747
Enseignement religieux 0527
Enseignement secondaire 0533
Enseignement spécial 0529
Enseignement supérieur 0745
Évaluation 0288
Finances 0277
Formation des enseignants 0530
Histoire de l'éducation 0520
Langues et littérature 0279
Lecture 0535
Mathématiques 0280
Musique 0522
Orientation et consultation 0519
Philosophie de l'éducation 0998
Physique 0523
Programmes d'études et enseignement 0727
Psychologie 0525
Sciences 0714
Sciences sociales 0534
Sociologie de l'éducation 0340
Technologie 0710

LANGUE, LITTÉRATURE ET LINGUISTIQUE
Langues
- Généralités 0679
- Anciennes 0289
- Linguistique 0290
- Modernes 0291

Littérature
- Généralités 0401
- Anciennes 0294
- Comparée 0295
- Mediévale 0297
- Moderne 0298
- Africaine 0316
- Américaine 0591
- Anglaise 0593
- Asiatique 0305
- Canadienne (Anglaise) 0352
- Canadienne (Française) 0355
- Germanique 0311
- Latino-américaine 0312
- Moyen-orientale 0315
- Romane 0313
- Slave et est-européenne 0314

PHILOSOPHIE, RELIGION ET THÉOLOGIE
Philosophie 0422
Religion
- Généralités 0318
- Clergé 0319
- Études bibliques 0321
- Histoire des religions 0320
- Philosophie de la religion 0322

Théologie 0469

SCIENCES SOCIALES
Anthropologie
- Archéologie 0324
- Culturelle 0326
- Physique 0327

Droit 0398
Économie
- Généralités 0501
- Commerce-Affaires 0505
- Économie agricole 0503
- Économie du travail 0510
- Finances 0508
- Histoire 0509
- Théorie 0511

Études américaines 0323
Études canadiennes 0385
Études féministes 0453
Folklore 0358
Géographie 0366
Gérontologie 0351
Gestion des affaires
- Généralités 0310
- Administration 0454
- Banques 0770
- Comptabilité 0272
- Marketing 0338

Histoire
- Histoire générale 0578
- Ancienne 0579
- Médiévale 0581
- Moderne 0582
- Histoire des noirs 0328
- Africaine 0331
- Canadienne 0334
- États-Unis 0337
- Européenne 0335
- Moyen-orientale 0333
- Latino-américaine 0336
- Asie, Australie et Océanie 0332

Histoire des sciences 0585
Loisirs 0814
Planification urbaine et régionale 0999
Science politique
- Généralités 0615
- Administration publique 0617
- Droit et relations internationales 0616

Sociologie
- Généralités 0626
- Aide et bien-àtre social 0630
- Criminologie et établissements pénitentiaires 0627
- Démographie 0938
- Études de l' individu et de la famille 0628
- Études des relations interethniques et des relations raciales 0631
- Structure et développement social 0700
- Théorie et méthodes. 0344
- Travail et relations industrielles 0629

Transports 0709
Travail social 0452

SCIENCES ET INGÉNIERIE

SCIENCES BIOLOGIQUES
Agriculture
- Généralités 0473
- Agronomie. 0285
- Alimentation et technologie alimentaire 0359
- Culture 0479
- Élevage et alimentation 0475
- Exploitation des péturages 0777
- Pathologie animale 0476
- Pathologie végétale 0480
- Physiologie végétale 0817
- Sylviculture et faune 0478
- Technologie du bois 0746

Biologie
- Généralités 0306
- Anatomie 0287
- Biologie (Statistiques) 0308
- Biologie moléculaire 0307
- Botanique 0309
- Cellule 0379
- Écologie 0329
- Entomologie 0353
- Génétique 0369
- Limnologie 0793
- Microbiologie 0410
- Neurologie 0317
- Océanographie 0416
- Physiologie 0433
- Radiation 0821
- Science vétérinaire 0778
- Zoologie 0472

Biophysique
- Généralités 0786
- Medicale 0760

SCIENCES DE LA TERRE
Biogéochimie 0425
Géochimie 0996
Géodésie 0370
Géographie physique 0368
Géologie 0372
Géophysique 0373
Hydrologie 0388
Minéralogie 0411
Océanographie physique 0415
Paléobotanique 0345
Paléoécologie 0426
Paléontologie 0418
Paléozoologie 0985
Palynologie 0427

SCIENCES DE LA SANTÉ ET DE L'ENVIRONNEMENT
Économie domestique 0386
Sciences de l'environnement 0768
Sciences de la santé
- Généralités 0566
- Administration des hipitaux 0769
- Alimentation et nutrition 0570
- Audiologie 0300
- Chimiothérapie 0992
- Dentisterie 0567
- Développement humain 0758
- Enseignement 0350
- Immunologie 0982
- Loisirs 0575
- Médecine du travail et thérapie 0354
- Médecine et chirurgie 0564
- Obstétrique et gynécologie 0380
- Ophtalmologie 0381
- Orthophonie 0460
- Pathologie 0571
- Pharmacie 0572
- Pharmacologie 0419
- Physiothérapie 0382
- Radiologie 0574
- Santé mentale 0347
- Santé publique 0573
- Soins infirmiers 0569
- Toxicologie 0383

SCIENCES PHYSIQUES
Sciences Pures
Chimie
- Genéralités 0485
- Biochimie 487
- Chimie agricole 0749
- Chimie analytique 0486
- Chimie minérale 0488
- Chimie nucléaire 0738
- Chimie organique 0490
- Chimie pharmaceutique 0491
- Physique 0494
- PolymÇres 0495
- Radiation 0754

Mathématiques 0405
Physique
- Genéralités 0605
- Acoustique 0986
- Astronomie et astrophysique 0606
- Electronique et électricité 0607
- Fluides et plasma 0759
- Météorologie 0608
- Optique 0752
- Particules (Physique nucléaire) 0798
- Physique atomique 0748
- Physique de l'état solide 0611
- Physique moléculaire 0609
- Physique nucléaire 0610
- Radiation 0756

Statistiques 0463

Sciences Appliqués Et Technologie
Informatique 0984
Ingénierie
- Généralités 0537
- Agricole 0539
- Automobile 0540
- Biomédicale 0541
- Chaleur et ther modynamique 0348
- Conditionnement (Emballage) 0549
- Génie aérospatial 0538
- Génie chimique 0542
- Génie civil 0543
- Génie électronique et électrique 0544
- Génie industriel 0546
- Génie mécanique 0548
- Génie nucléaire 0552
- Ingénierie des systämes 0790
- Mécanique navale 0547
- Métallurgie 0743
- Science des matériaux 0794
- Technique du pétrole 0765
- Technique minière 0551
- Techniques sanitaires et municipales 0554
- Technologie hydraulique 0545

Mécanique appliquée 0346
Géotechnologie 0428
Matières plastiques (Technologie) 0795
Recherche opérationnelle 0796
Textiles et tissus (Technologie) 0794

PSYCHOLOGIE
Généralités 0621
Personnalité 0625
Psychobiologie 0349
Psychologie clinique 0622
Psychologie du comportement 0384
Psychologie du développement 0620
Psychologie expérimentale 0623
Psychologie industrielle 0624
Psychologie physiologique 0989
Psychologie sociale 0451
Psychométrie 0632

THE UNIVERSITY OF CALGARY

FACULTY OF GRADUATE STUDIES

The undersigned certify that they have read, and recommend to the Faculty of Graduate Studies for acceptance, a thesis entitled *Frequency Response Phase Estimation of the UHF Indoor Communications Channel* submitted by Brian Paul Donaldson in partial fulfillment of the requirements for the degree of Master of Engineering.

Michel Fattouche

Supervisor: Dr. M. Fattouche
Department of Electrical and Computer Engineering

Dr. A. Sesay
Department of Electrical and Computer Engineering

Dr. G. Lachapelle
Department of Geomatics Engineering

March 24, 1993

ABSTRACT

In recent years the attention focused on UHF indoor wireless communication systems has dramatically increased. Consequently there is a growing demand for simple, cost effective, and accurate indoor channel characterization methods. The recent introduction of indoor frequency domain measurement systems has made possible accurate channel characterization, but the systems are complex and expensive.

This thesis shows that it is possible to calculate wideband response parameters, specifically the root mean square delay spread τ_{rms}, with knowledge of the indoor channel's frequency response magnitude spectrum only. Application of this result makes possible a simple, inexpensive, and accurate wideband channel characterization system using equipment commonly found in an RF research facility. The apparent frequency dependent nature of τ_{rms} is also discussed.

PREFACE

To aid in the study of UHF indoor communications channel characterization, 12,000 frequency domain measurements were taken in 1991. This author uses some of the data to measure the channel's wideband response and make conclusions with respect to the channel's minimum phase properties and frequency dependent nature. These results, as well as possible industry applications, are presented in Chapters Four through Six of this thesis; the necessary background is provided in the first three chapters. A brief summary of each chapter follows.

Chapter One introduces the indoor communications channel and the parameters used to characterize its wideband response.

Chapter Two describes the frequency domain measurement system and the experimental indoor channel. The treatment of the data and post-processing issues such as data windowing are also discussed.

A theoretical background is presented in Chapter Three. Topics covered include the RMS delay spread, the z-transform, system causality, and minimum phase systems.

Chapter Four examines the causality of the experimental channel. The results of this chapter are used to verify the measurement system and provide a basis for the discussions in Chapter Five.

Chapter Five investigates the accuracy of the RMS delay spread estimates. Environmental influences on the indoor channel are also discussed.

The results are summarized and concluded in Chapter Six and potential future research projects are suggested.

ACKNOWLEDGMENTS

I would like to thank my supervisor, Dr. Michel Fattouche, for his keen interest and help throughout. I especially appreciate his continued dedication while on sabbatical.

Affectionately dedicated to Linda

for her support and encouragement

CONTENTS

LIST OF FIGURES

LIST OF SYMBOLS AND ABBREVIATIONS

Symbols

α_t	Student's *t*-statistic
α_n	Envelope of (n+1)st path
γ_t	Sampling rate (time domain)
γ_f	Sampling rate (frequency domain)
$\delta(\cdot)$	Kronecker delta function
Δ	Aperture width
Δf	Frequency separation between successive samples
ε	Energy
λ	Wavelength
τ_{m}	Mean excess delay
τ_{rms}	RMS delay spread
$\tilde{\tau}_{\mathrm{rms}}$	Estimation of RMS delay spread
$\Psi[\cdot]$	Hilbert transform operator
ω	Angular frequency
B_c	Coherence bandwidth
c	Speed of light
D_1	Horizontal distance from light source to aperture plane
D_2	Horizontal distance from screen to aperture plane
f	Frequency
f_c	Critical (Nyquist) frequency
f_n	Frequency of (n+1)st sample

$h(n)$ Impulse response at (n+1)st sample

$\tilde{h}(n)$ Estimation of impulse response at (n+1)st sample

$H(e^{j\omega})$ Channel transfer function

$H(f)$ Channel transfer function

$\tilde{H}(e^{j\omega})$ Estimation of channel transfer function

$H(z)$ z-transform of $h(n)$

$\hat{H}(z)$ Complex natural logarithm of $H(z)$

$h_s(n)$ Conjugate symmetric function

$h_a(n)$ Conjugate antisymmetric function

$H_I(e^{j\omega})$ Real part of channel transfer function

$H_R(e^{j\omega})$ Imaginary part of channel transfer function

I Light intensity

I_0 Light intensity (no diffraction)

j $\sqrt{-1}$

r Linear correlation coefficient

r^2 Coefficient of determination

$\mathrm{sgn}(\cdot)$ Signum function

t Time

t_c Critical time

t_n Arrival time of (n+1)st path

T_S Time separation between successive samples

$W(f)$ Window function

$X(f_n)$ Channel frequency response to (n+1)st sample

$\{\cdot\}$ Sequence template

$\Leftrightarrow$ Fourier transform pair

Abbreviations

dB	Decibel
EM	Electromagnetic
FFT	Fast Fourier transform
IDFT	Inverse discrete Fourier transform
LAN	Local area network
LOS	Line of sight
NLOS	Non-line of sight
RF	Radio frequency
RMS	Root mean square
SNR	Signal-to-noise ratio
UHF	Ultrahigh frequency

Multiplier Prefixes

n	nano	$\cdot 10^{-9}$
μ	micro	$\cdot 10^{-6}$
m	milli	$\cdot 10^{-3}$
c	centi	$\cdot 10^{-2}$
k	kilo	$\cdot 10^{3}$
M	mega	$\cdot 10^{6}$
G	giga	$\cdot 10^{9}$

CHAPTER ONE

Introduction

In recent years the attention focused on indoor wireless communication systems has dramatically increased. This increase can be largely attributed to the advance in popularity and availability of indoor services such as wireless LANs and cordless telephones.

A necessary step in the development cycle of an indoor communications product is the characterization of its target channel. Channel parameters such as coherence bandwidth, excess delay, and root mean square (RMS) delay spread are often required. These parameters are obtained by measuring the wideband response of the channel.

1.1 History of Indoor Wideband Measurements

Prior to 1984 very little indoor channel characterization research had been conducted. Devasirvatham was the first to characterize the indoor channel using wideband measurements [Devasirvatham, 1984]; Bultitude extended Devasirvatham's research in 1987 [Bultitude, 1987]. During the middle to late 1980's almost all indoor wideband measurements were made exclusively in the time domain. It wasn't until Pahlavan and Howard introduced a frequency domain measurement system in 1989 that such systems started gaining notoriety [Pahlavan and Howard, 1989]. Molkdar reported that all wideband measurements prior to 1991 had been conducted in the time domain [Molkdar, 1991]. Although Molkdar's claim is incorrect, it does underscore the rarity of frequency domain measurements during that time period. In 1991 Morrison unveiled an indoor frequency domain measurement system capable of both narrowband and wideband measurements [Morrison]. It seems probable that the popularity of frequency domain measurement systems will continue to increase.

When measuring the indoor channel's frequency response, researchers have assumed that both its magnitude and phase are required to accurately express the channel's wideband characteristics. This thesis shows that it is possible to calculate one of the most popular wideband response parameters, namely the RMS delay spread τ_{rms}, by measuring only the magnitude of the channel's frequency response. Some researchers have reported a relationship between τ_{rms} and the test signal's path length [Devasirvatham, 1986; Zaghloul *et al.*, 1990] while others have not [Rappaport, 1989; Saleh and Valenzuela, 1987]. This phenomenon remains unexplained to date. A relationship between signaling frequency and τ_{rms} has also been noted [Morrison, pg. 83; Zaghloul *et al.*, 1991] but is still unexplained. Causes of the apparent frequency dependent nature of τ_{rms} are explored in this thesis.

1.2 Indoor Channel Characterization

The indoor environment is a fading multipath channel. The scattering and reflective nature of the environment causes multiple propagation paths between transmitter and receiver. Associated with each path is a difference in path length and a corresponding propagation delay. One characteristic of a multipath channel is the time spread of a transmitter's signal; when measured at the receiver the time spread is called the *excess delay*.

In addition to creating an excess delay, the multipath components give rise to *signal fading*, i.e., a fade in the magnitude of the channel's frequency response. This occurs when the phases of the individual paths add destructively. A small variation in the path difference can cause a substantial phase difference since

$$\frac{\text{phase difference}}{2\pi} = \frac{\text{path difference}}{\lambda} \tag{1.1}$$

where λ is the signal's wavelength. For example, a 1 GHz signal shifts 180° when its path difference is 1.67 m.

In general, the indoor channel changes with time. Its response to a signal is therefore a function of its time dependent multipath components. The *impulse response*, i.e., the channel's response to a very short pulse, is given by the following expression [Proakis, pg. 704].

$$h(\tau,t) = \sum_{n=0}^{N-1} \alpha_n(t) e^{-j\theta_n(t)} \delta[\tau - \tau_n(t)] \tag{1.2}$$

where $h(\tau,t)$ is the impulse response at delay τ and time instant t,

$\alpha_n(t)$ is the amplitude of the nth path,

$\theta_n(t)$ is the phase of the nth path,

$\tau_n(t)$ is the propagation delay of the nth path,

and N is the number of paths.

The *multipath intensity profile* is the square of the impulse response's magnitude; it is the relative power of the multipath components.

1.2.1 Wideband Response Parameters

Two sinusoids with a frequency separation greater than a channel's *coherence bandwidth* are affected differently by the channel. The coherence bandwidth B_c is inversely proportional to the channel's RMS delay spread τ_{rms}. In practice, the constant of proportionality is close to unity so that

$$B_c \approx \frac{1}{\tau_{\mathrm{rms}}} \tag{1.3}$$

Wideband channel measurements are of interest when the system's bandwidth exceeds B_c.

Of the wideband response parameters, the RMS delay spread is used most frequently to characterize a channel. τ_{rms} is the standard deviation of the multipath intensity profile; it is an important parameter as it is used in determining the maximum signaling bandwidth for a given error rate [Jakes, pp. 236-240]. When the channel is stationary, the following equations define τ_{rms} [Morrison, pp. 8-9].

$$\tau_{\mathrm{rms}} = \left[\frac{\sum_{n=0}^{N-1} \left(t_n - \tau_{\mathrm{m}} - t_0\right)^2 \alpha_n^2}{\sum_{n=0}^{N-1} \alpha_n^2} \right]^{1/2} \tag{1.4}$$

where t_n is the arrival time of the $(n + 1)$st path,

α_n is the envelope of the $(n + 1)$st path,

and N is the number of multipath components.

The *mean excess delay* τ_{m} is

$$\tau_{\mathrm{m}} = \frac{\sum_{n=0}^{N-1} \left(t_n - t_0\right) \alpha_n^2}{\sum_{n=0}^{N-1} \alpha_n^2} \tag{1.5}$$

Indoor channel frequency domain measurement systems have recently become available. Using such a system, τ_{rms} is calculated by transforming the frequency domain data into the time domain to obtain the impulse response; the impulse response is then used in Equations (1.4) and (1.5). Both the magnitude and phase of the transfer function are required to calculate the impulse response. Currently it is assumed that in order to calculate τ_{rms}, the frequency domain measurement system must record both the magnitude and phase of the frequency response. The following chapters show that for the indoor channel, τ_{rms} may be calculated with knowledge of the (measured) transfer function's magnitude only.

1.2.2 Thesis Outline

This thesis is comprised of six chapters. Chapters Two and Three provide necessary background information; Chapters Four and Five describe and analyze experimental results; a summary and conclusions are presented in Chapter Six. A brief summary of Chapters Two through Six follows.

Chapter Two describes the frequency domain measurement system and the experimental indoor channel. The treatment of the data and post-processing issues such as data windowing are also discussed.

A theoretical background is presented in Chapter Three. Topics covered include the RMS delay spread, the *z*-transform, system causality, and minimum phase systems.

Chapter Four examines the causality of the experimental channel. The results of this chapter are used to verify the measurement system and provide a basis for the discussions in Chapter Five.

Chapter Five investigates the accuracy of the RMS delay spread estimates. Environmental influences on the indoor channel are also discussed.

The results are summarized and concluded in Chapter Six and potential future research projects are suggested.

CHAPTER TWO

The Measurement System and Experimental Data

This chapter describes the frequency domain measurement system and the data obtained through its use. The system and data were used by Gerald Morrison for his Master of Science thesis. A detailed description of the system is given in Chapter Two of Morrison's thesis [Morrison, pp. 18-48].

2.1 The Frequency Domain Measurement System

Morrison constructed a frequency domain measurement system using a network analyzer with an S-parameter test set, an amplifier, cables, two antennas, and a personal computer. This basic configuration is shown in Figure 2.1.

The HP8753A Vector Network Analyzer is capable of measuring both the magnitude and phase of a linear network's transfer function. Wideband measurements from 300 kHz to 3 GHz are possible. The indoor RF propagation channel's transfer function is measured by placing the transmit and receive antennas somewhere in the indoor environment. The network analyzer sweeps the channel by transmitting a sine wave of increasing frequency and measuring the received response. The starting frequency f_0, the stopping frequency f_{N-1}, and the frequency separation between successive samples Δf, are all determined by the user. For example, to obtain a transfer function with bandwidth $N \cdot \Delta f$, $N = (f_{N-1} - f_0) / \Delta f$ samples are required. The channel's transfer function $H(f)$ is

$$H(f) = \sum_{n=0}^{N-1} X(f_n)\delta(f_n - f_0 - n \cdot \Delta f), \quad f_0 \le f \le f_{N-1} \tag{2.1}$$

where $X(f_n)$ is the channel's frequency response to the (n+1)st sample and

$$\delta(n) = \begin{cases} 1, & n = 0 \\ 0, & n \neq 0 \end{cases} \tag{2.2}$$

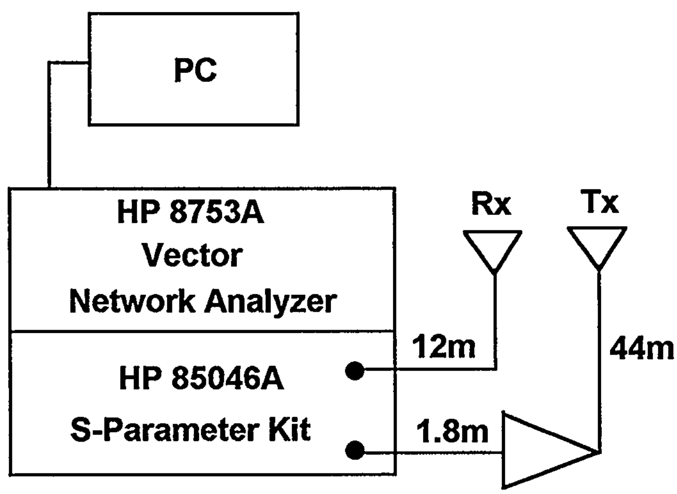

Fig. 2.1: Measurement System Configuration

2.2 Data Collection

An experimental channel was constructed by using the frequency domain measurement system inside a modern office building. The transmit and receive antennas were placed in a hallway with an unobstructed line of sight (LOS) between them. A solid wall completely closed off one side of the hallway; the other side was partially blocked with portable office partitions. The antennas were setup approximately one metre from the solid wall. This *experimental channel* (hereafter referred to as such) is diagrammed in Figure 2.2.

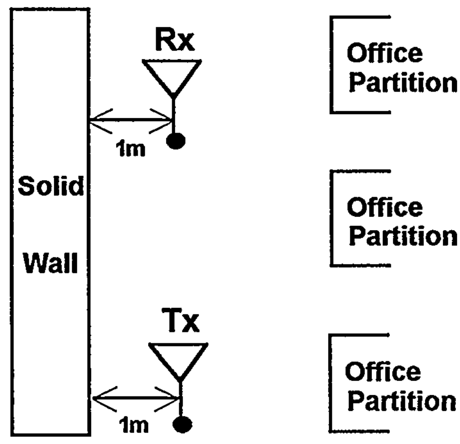

Fig. 2.2: The Experimental Channel

Various frequency response measurements were taken focusing primarily on two criteria: the distance between the antennas and the centre of frequency of the sweep. To ensure channel stationarity the measurements were taken during building quiet times.

2.2.1 Distance-Oriented Measurements

Distance-oriented measurements were performed to determine the experimental channel's transfer function at various antenna separations. The measurements were in two, 200 MHz bands centred at 1000 MHz and 1600 MHz. Data were collected for transmitter-receiver separations of 0.5 m to 30 m in 0.5 m increments. At each separation, ten frequency responses which contained 255 uniformly spaced points each were collected and averaged. The frequency resolution of the samples was therefore 784 kHz; a LOS path was maintained throughout the data collection process.

2.2.2 Frequency-Oriented Measurements

The frequency-oriented measurements were performed twice - first using a LOS path and then using an obstructed (NLOS) path. An obstruction was created by placing a bookshelf between the two antennas. A total of fifty data sets (25 LOS and 25 NLOS) were collected for transmitter-receiver separations of 11 m to 12 m in 4 cm increments. At each separation, ten frequency responses which contained 2401 uniformly spaced points each were collected and averaged. The frequency sweep was from 1000 MHz to 2500 MHz thus providing a frequency resolution of 625 kHz per sample.

In order to analyze the data it is necessary to take its inverse discrete Fourier transform (see Section 2.3). Since it is not practical to do so for large data sets, the data were processed 256 points at a time. After the first 256 points were processed, a sliding window was moved by 32 points and the next 256 points were processed, and so on, for all 2401 points. The resulting bandwidth of each data set was therefore 160 MHz; the frequency centre of the nth data set was $1080\,\text{MHz} + (n-1)\cdot 160\,\text{MHz}$. In some cases, time domain data with the same frequency centre were averaged across all twenty-five LOS or NLOS data sets. This was done to effectively remove any distance-oriented influence and highlight any frequency-oriented influence. The treatment and analysis of the data are detailed in Chapters Four and Five.

2.3 Data Post-Processing

If frequency domain data analysis is required the data may be used directly, i.e., it may not be necessary to post-process the data. In order to obtain the experimental channel's RMS delay spread, however, it is necessary to transform the data into the time domain. The time domain equivalent to the transfer function is the impulse response, which is obtained from the transfer function via the inverse discrete Fourier transform (IDFT). Efficient fast Fourier transform (FFT) algorithms are available and can be used to compute the IDFT.

In order to ensure that the FFT algorithms produce acceptable results, care must be taken to safeguard against *aliasing* and/or *leakage*. Aliasing can occur if the resolution of the sampled data is not sufficiently granular; leakage can occur if an inappropriate data windowing function is used.

2.3.1 Time Domain Aliasing

Aliasing is commonly associated with sampled time domain data that have been transformed into the frequency domain. If the time domain sampling rate is not sufficiently fast then after transformation into the frequency domain, high frequency components are aliased to appear as lower frequency components. The sampling theorem makes explicit the relationship between the time domain sampling rate γ_t (where γ_t has units samples/s) and the *Nyquist* or *critical frequency* f_c. The critical frequency is the frequency at which aliasing begins. The sampling theorem states that

$$\gamma_t = 2f_c \tag{2.3}$$

If the signal $x(t)$ being sampled is bandlimited to contain no frequency components greater than f_b, then no aliasing will occur provided that

$$\gamma_t \geq 2f_b \tag{2.4}$$

where $X(f) = 0, \ |f| > f_b$

and $X(f)$ is the Fourier transform of $x(t)$.

The data described in Section 2.2 were collected in the frequency domain. Associated with frequency domain data collection is the frequency domain sampling rate γ_f, where γ_f has units samples/Hz. For frequency domain sampling, Equation (2.3) becomes

$$\gamma_f = 2t_c \tag{2.5}$$

where t_c is the *critical time.*

Since it is the channel's transfer function that is being sampled, the corresponding time domain representation is the impulse response. In this case, t_c is the RMS delay spread of the channel. If Δf is the separation between the frequency domain samples, then to avoid time domain aliasing

$$\frac{1}{\Delta f} \geq 2\,\tau_{\mathrm{rms}} \tag{2.6}$$

where $\gamma_f = \frac{1}{\Delta f}$.

The RMS delay spread of the experimental channel is less than 100 ns, hence, Δf should be less than 5 MHz to avoid aliasing. The frequency separation of the data was well within this bound.

2.3.2 Data Windowing

The data collected by the frequency domain measurement system were bandlimited between f_0 and f_{N-1}. Hence the measured transfer function $H(f)$ can be described as

$$H(f) = \begin{cases} X(f_n), & f = f_n \\ 0, & \text{elsewhere} \end{cases} \tag{2.7}$$

where $X(f_n)$ is the channel's frequency response to the (n+1)st sample,

$f_n = f_0 + n \cdot \Delta f, \quad n = 0, 1, \ldots, N-1,$

and N is the number of samples.

Equivalently, $H(f)$ can be interpreted as a windowed portion of $X(f_n)$, i.e.,

$$H(f) = X(f_n) W_{\mathrm{rect}}(f) \tag{2.8}$$

where

$$W_{\mathrm{rect}}(f) = \begin{cases} 1, & f_0 \le f \le f_{N-1} \\ 0, & \text{elsewhere} \end{cases} \tag{2.9}$$

is the rectangular *window function*. When transformed to the time domain, the impulse response $h(n)$ becomes

$$h(n) = x(t) * w_{\mathrm{rect}}(t) \tag{2.10}$$

where the asterisk denotes complex convolution and the inverse Fourier transform of $W_{\mathrm{rect}}(f)$ is the rectangular *leakage function* $w_{\mathrm{rect}}(t)$ given by

$$w_{\mathrm{rect}}(t) = \frac{\sin\left(\frac{N}{2} t\right)}{\sin\left(\frac{1}{2} t\right)} \tag{2.11}$$

where t is periodic in 2π

and $h(n)$ spans one *bin*, i.e., $2\pi n / N \le t < 2\pi(n+1)/N, \quad n = 0, 1, \ldots, N-1.$

Ideally, $w_{\mathrm{rect}}(t)$ would be a Dirac delta pulse so that $h(n) = x(t)$. However, $w_{\mathrm{rect}}(t)$ is a modified sinc function and hence convolving $x(t)$ with $w_{\mathrm{rect}}(t)$ results in power from adjacent bins leaking into $h(n)$; for example, $h(n)$ will contain some aliased power from $h(n+1)$. The rectangular leakage function is shown in Figure 2.3.

The design of a window function that has a corresponding well behaved leakage function has been the focus of many research endeavors; the three term Blackman-Harris window [Harris, 1978] is a result of such research. The Blackman-Harris leakage function $w_{\mathrm{bh}}(t)$ is constructed by adding weighted shifts of $w_{\mathrm{rect}}(t)$ as follows (see Figure 2.4).

$$w_{\mathrm{bh}}(t) = a_0 w_{\mathrm{rect}}(t) + \frac{a_1}{2}\left[w_{\mathrm{rect}}(t + \tfrac{2\pi}{N}) + w_{\mathrm{rect}}(t - \tfrac{2\pi}{N})\right] + \frac{a_2}{2}\left[w_{\mathrm{rect}}(t + \tfrac{4\pi}{N}) + w_{\mathrm{rect}}(t - \tfrac{4\pi}{N})\right] \tag{2.12}$$

where $a_0 = 0.42323$,

$a_1 = 0.49755$,

and $a_2 = 0.07922$.

The Blackman-Harris window function $W_{\mathrm{bh}}(f)$ (Figure 2.5) is the Fourier transform of $w_{\mathrm{bh}}(t)$, i.e.,

$$W_{\mathrm{bh}}(f) = a_0 - a_1 \cos\left(\tfrac{2\pi n}{N}\right) + a_2 \cos\left(\tfrac{4\pi n}{N}\right), \quad n = 0,1,\ldots,N-1 \tag{2.13}$$

Choosing a particular window function is essentially a tradeoff between making the *resolving bandwidth* (i.e., the width of the mainlobe 6 dB below its peak) of the leakage function as narrow as possible versus making the sidelobes of the leakage function fall off as rapidly as possible [Press *et al.*, pp. 441-444]. A wide mainlobe causes loss of resolution in the time domain whereas large sidelobes cause leakage. The Blackman-Harris window is thought to employ a reasonable tradeoff. The log magnitude of the rectangular and Blackman-Harris leakage functions are compared in Figure 2.6.

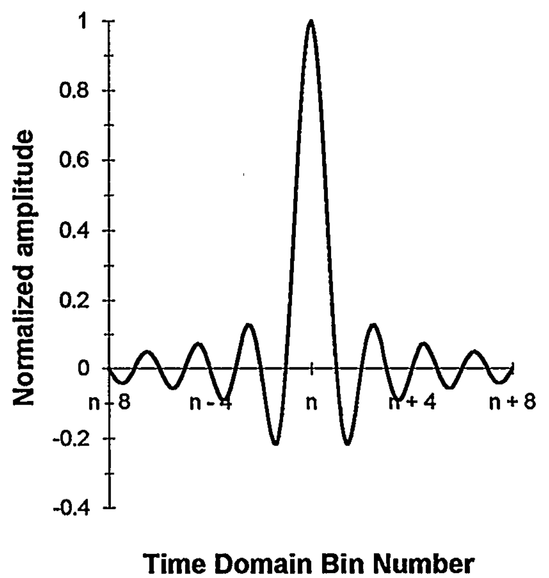

Fig. 2.3: Rectangular Leakage Function

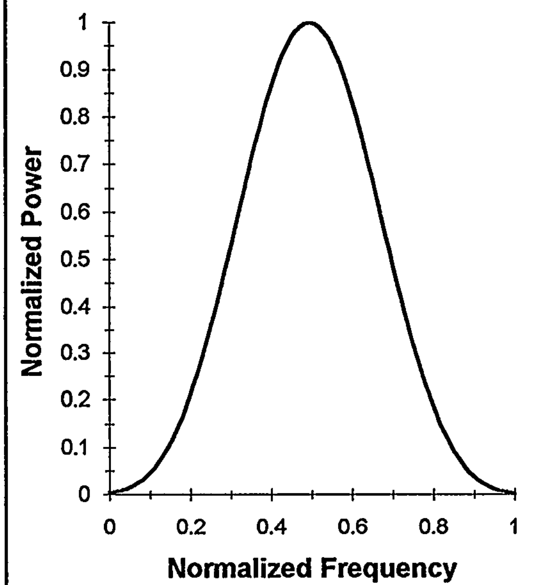

Fig. 2.5: The Blackman-Harris Window Function

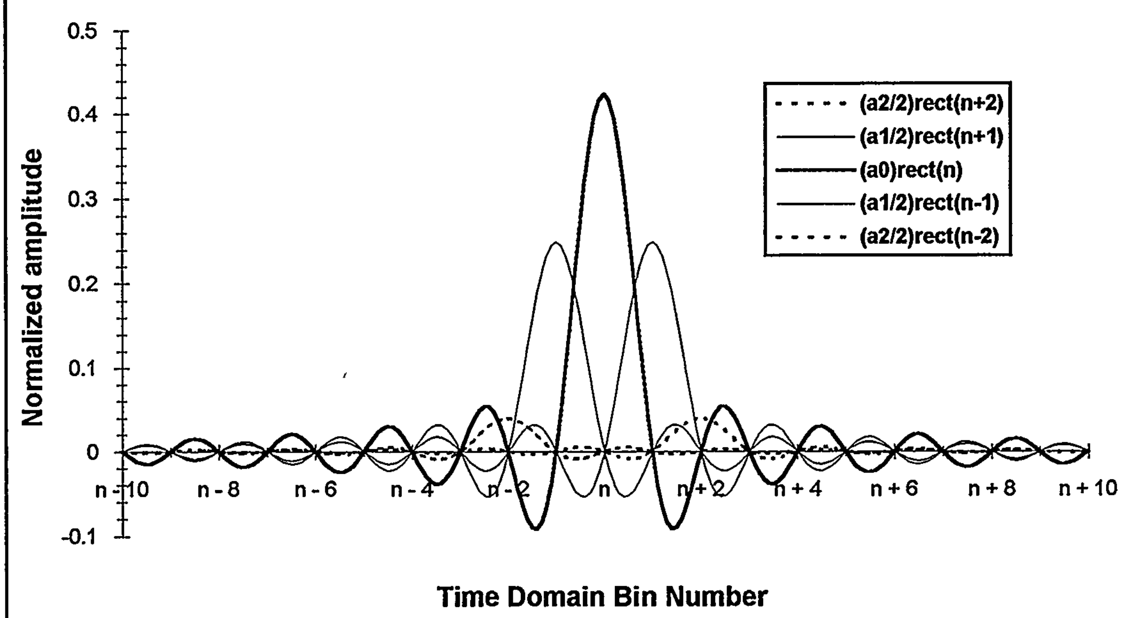

Fig. 2.4: Construction of Blackman-Harris Leakage Function

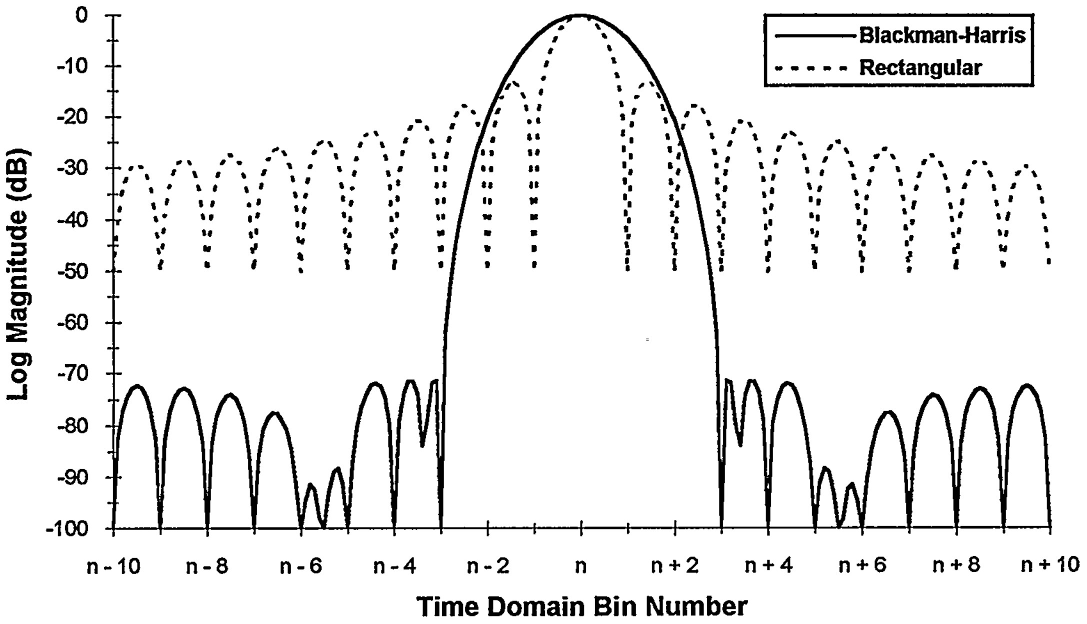

Fig. 2.6: Rectangular and Blackman-Harris Leakage Functions

CHAPTER THREE

Theoretical Background

A channel's RMS delay spread is a characterization of its multipath environment; it is a function of the channel's impulse response. The impulse response is obtainable with knowledge of the channel's transfer function. In general, both the magnitude and phase of the transfer function must be known. However, if the channel is *minimum phase* it is possible to calculate its impulse response, accurate to within a constant time shift, with knowledge of the transfer function's magnitude spectrum only. The constant shift in time does not affect τ_{rms}. The calculation of τ_{rms} under general and minimum phase conditions is discussed in this chapter.

3.1 RMS Delay Spread

When discrete measurements of a channel's transfer function are available, its impulse response may be calculated via the IDFT, i.e.,

$$h(n) = \frac{1}{N}\sum_{k=0}^{N-1} H(e^{j\omega_k})e^{j2\pi kn/N}, \qquad 0 \le n \le N-1 \tag{3.1}$$

where N is the number of frequency-domain samples,

$H(e^{j\omega_k})$ is the frequency response at $(k \cdot \Delta f + f_0)$ Hz,

Δf is the frequency separation between $H(e^{j\omega_k})$ and $H(e^{j\omega_{k+1}})$,

f_0 is the frequency of the first sample $H(e^{j\omega_0})$,

$h(n)$ is the impulse response at time nT_s,

and $T_s = (N \cdot \Delta f)^{-1}$ is the time separation between $h(n)$ and $h(n+1)$.

If the channel is *causal* then $h(n) = 0$ for $n < 0$. Due to the periodic nature of the IDFT, however, the causality criterion is equivalent to $h(n) = 0$ for $N/2 \le n \le N-1$. The RMS delay spread of a causal channel becomes [from Equations (1.4) and (1.5)]:

$$\tau_{\mathrm{rms}} = \left[\frac{\sum_{n=0}^{N/2-1} (nT_s - \tau_{\mathrm{m}} - aT_s)^2 |h(n)|^2}{\sum_{n=0}^{N/2-1} |h(n)|^2} \right]^{1/2} \tag{3.2}$$

and

$$\tau_{\mathrm{m}} = \left[\frac{\sum_{n=0}^{N/2-1} (n-a)T_s |h(n)|^2}{\sum_{n=0}^{N/2-1} |h(n)|^2} \right]^{1/2} \tag{3.3}$$

where the (a+1)st sample is the first arrival.

Conditions under which τ_{rms} may be calculated with knowledge of only $|H(e^{j\omega})|$ are discussed in Subsection 3.4.2.

3.2 The *z*-Transform

The *z*-transform $H(z)$ of the impulse response of a discrete-time, linear, shift-invariant system is defined as

$$H(z) = \sum_{n=-\infty}^{\infty} h(n) z^{-n} \tag{3.4}$$

where z is a complex number. For $z = e^{j\omega}$, i.e., points on the unit circle of the z-plane,

$$H(e^{j\omega}) = \sum_{n=-\infty}^{\infty} h(n) e^{-j\omega n} \tag{3.5}$$

which is the discrete Fourier transform of $h(n)$.

When $h(n)$ is a discrete, stable, and causal sequence of finite-length N, $H(z)$ is a N-1 degree polynomial in z^{-1} with all poles at the origin. For $H(e^{j\omega})$ to exist, the region of convergence of $H(z)$ must include the unit circle. To see that the region of convergence is the exterior of a circle whose radius is less than unity, suppose that

$$\sum_{n=0}^{N-1} \left| h(n) z_1^{-n} \right| < \infty \tag{3.6}$$

If $|z| > |z_1|$ then

$$\left| h(n) z^{-n} \right| < \left| h(n) z_1^{-n} \right|, \quad 0 < n \le N-1 \tag{3.7}$$

and thus

$$\sum_{n=0}^{N-1} \left| h(n) z^{-n} \right| < \infty, \quad |z| > |z_1| \tag{3.8}$$

Since $h(n)$ is *stable*

$$\sum_{n=0}^{N-1} |h(n)| < \infty \tag{3.9}$$

and hence Equation (3.6) is true when $|z_1| \geq 1$, i.e., the region of convergence is a circle of radius less than one.

To summarize, the z-transform of a discrete, stable, and causal sequence of finite-length N has a region of convergence that is the exterior of a circle with radius less than one; its N-1 poles are all at the origin while the N-1 zeros may be located anywhere. A stable system is causal if and only if the poles of its z-transform are all inside the unit circle.

3.3 Causal Systems

A system is *causal* if and only if its impulse response $h(n)$ is zero for $n < 0$. However, it is not necessary to obtain $h(n)$ to determine whether or not a system is causal. The following shows that the imaginary part of $H(e^{j\omega})$ is the *Hilbert transform* of the real part of $H(e^{j\omega})$ if and only if the system is stable and causal.

A *conjugate symmetric sequence* $\{h_s(n)\}$ is a sequence for which $\{h_s(n)\} = \{h_s^*(-n)\}$; a *conjugate antisymmetric sequence* $\{h_a(n)\}$ has the property that $\{h_a(n)\} = \{-h_a^*(-n)\}$. Any sequence $\{h(n)\}$ can be expressed as the sum of a conjugate symmetric sequence and a conjugate antisymmetric sequence, i.e.,

$$h(n) = h_s(n) + h_a(n) \tag{3.10}$$

where

$$h_s(n) = \tfrac{1}{2}\left[h(n) + h^*(-n)\right] \tag{3.11}$$

and

$$h_a(n) = \tfrac{1}{2}\left[h(n) - h^*(-n)\right] \tag{3.12}$$

$\{h_s(n)\}$ and $\{h_a(n)\}$ are related to $H(e^{j\omega})$ by the identities

$$h_s(n) \Leftrightarrow H_R(e^{j\omega}) \tag{3.13}$$

and

$$h_a(n) \Leftrightarrow jH_I(e^{j\omega}) \tag{3.14}$$

where $H_R(e^{j\omega})$ is the real part of $H(e^{j\omega})$,

$H_I(e^{j\omega})$ is the imaginary part of $H(e^{j\omega})$,

and $\Leftrightarrow$ denotes a Fourier transform pair.

If (and only if) $h(n)$ is causal, then $h_s(n)$ and $h_a(n)$ are related such that

$$h_a(n) = h_s(n)\,\mathrm{sgn}(n) \tag{3.15}$$

where

$$\mathrm{sgn}(n) = \begin{cases} -1, & n < 0 \\ 1, & n > 0 \end{cases} \tag{3.16}$$

The result of multiplying both sides of Equation (3.15) by *-j* and taking its Fourier transform is

$$H_I(e^{j\omega}) = H_R(e^{j\omega}) * \left(-\frac{2}{\omega}\right) \tag{3.17}$$

Equation (3.17) defines a *Hilbert transform* relation, i.e.,

$$H_I(e^{j\omega}) = \Psi\left[H_R(e^{j\omega})\right] \tag{3.18}$$

where $\Psi[\cdot]$ denotes the Hilbert transform.

Equation (3.18) suggests that it is possible to determine whether or not a system is causal by comparing the imaginary part of its transfer function against the Hilbert transform of the real part of its transfer function. The system is causal if and only if Equation (3.18) is satisfied.

3.4 Minimum Phase Systems

A stable and causal system is *minimum phase* if and only if the zeros of its *z*-transform are all inside the unit circle. Recall that (Section 3.2) if $h(n)$ is a discrete, stable, and causal sequence of finite-length *N*, then $H(z)$ contains *N*-1 poles at the origin and *N*-1 zeros, all of which are not necessarily inside the unit circle.

A zero of $H(z)$ may be reflected to its conjugate reciprocal location without changing the magnitude of the system's *z*-transform. The *conjugate reciprocal* of z_0 is $1/z_0^*$, i.e., a zero located at $z = z_0$ will be located at $z = 1/z_0^*$ after it has been reflected. Since every zero is in one of two possible locations (either inside or outside the unit circle), a system with a given magnitude response $|H(z)|$ has 2^{N-1} possible phase curves $\arg[H(z)]$. To see that this is true, consider a stable and causal system $H(z)$ that has all of its zeros inside the unit circle except for a zero at $z = 1/z_0$, $|z_0| < 1$. $H(z)$ can be expressed as

$$H(z) = H_1(z)(z^{-1} - z_0) \tag{3.19}$$

where $H_1(z)$ contains all the zeros of $H(z)$ except the zero at $z = 1/z_0$, i.e., $H_1(z)$ is minimum phase. By multiplying the numerator and denominator of the right hand side of Equation (3.19) by $1 - z_0^* z^{-1}$, $H(z)$ becomes

$$H(z) = H_2(z) H_{ap}(z) \tag{3.20}$$

where

$$H_2(z) = H_1(z)(1 - z_0^* z^{-1}) \tag{3.21}$$

is minimum phase and

$$H_{ap}(z) = \frac{z^{-1} - z_0}{1 - z_0^* z^{-1}} \tag{3.22}$$

is *allpass* since

$$\begin{aligned} \left|H_{ap}(e^{j\omega})\right|^2 &= \left[\frac{e^{-j\omega} - z_0}{1 - z_0^* e^{-j\omega}}\right]\left[\frac{e^{j\omega} - z_0^*}{1 - z_0 e^{j\omega}}\right] \\ &= \frac{1 - z_0^* e^{-j\omega} - z_0 e^{j\omega} + |z_0|^2}{1 - z_0^* e^{-j\omega} - z_0 e^{j\omega} + |z_0|^2} \\ &= 1 \end{aligned} \tag{3.23}$$

$H_2(z)$ differs from $H(z)$ only in that the zero of $H(z)$ at $z = 1/z_0$ is reflected to $z = z_0^*$ in $H_2(z)$, i.e.,

$$|H_2(z)| = |H(z)| \tag{3.24}$$

but

$$\arg[H_2(z)] \neq \arg[H(z)] \tag{3.25}$$

in general. This shows that a stable and causal system with an impulse response of finite-length N has, in general, 2^{N-1} different phase curves for a given magnitude spectrum.

It is of interest to note [Robinson and Treitel, pg. 59; Oppenheim and Schafer, pg. 352] that the phase-lag spectrum of a system with all of its zeros inside the unit circle is a minimum with respect to the phase-lag spectra of the $2^{N-1}-1$ other members of that set (where the impulse response of the system is a sequence of length N). This suggests the reason for the term *minimum phase*, although *minimum phase lag* would be a more precise description. Similarly, a system with all of its zeros outside the unit circle has a maximum phase-lag spectrum and is therefore called *maximum phase*.

3.4.1 Minimum Delay Sequences

The *total energy* ε of a sequence $\{h(n)\}$ is defined as

$$\varepsilon = \sum_{n=-\infty}^{\infty} |h(n)|^2 \tag{3.26}$$

Consider a stable, causal system with an impulse response of finite length N. In general, there are 2^{N-1} different sequences of length N whose z-transform magnitude spectra are identical. These 2^{N-1} sequences are said to form a *suite* [Robinson and Treitel, pg. 114]. By Parseval's Theorem, the total energy of each sequence in the suite is identical, i.e.,

$$\varepsilon_i = \sum_{n=0}^{N-1} |h_i(n)|^2 = \frac{1}{2\pi}\int_{-\pi}^{\pi} \left|H_i\left(e^{j\omega}\right)\right|^2 d\omega = \varepsilon, \quad i = 0,1,\ldots,2^{N-1}-1 \tag{3.27}$$

The *partial energy* $\varepsilon(m)$ of a sequence $\{h(n)\}$ is the energy contributed by the first m+1 samples in the sequence, i.e.,

$$\varepsilon(m) = \sum_{n=0}^{m} |h(n)|^2, \quad m = 0,1,\ldots,N-1 \tag{3.28}$$

A *minimum delay sequence* can therefore be defined as a sequence in a suite whose partial energy is never less than the partial energy of any sequence in the suite. Hence,

$$\varepsilon(m) \geq \varepsilon_i(m), \quad i = 0,1,\ldots,2^{N-1}-1; \; m = 0,1,\ldots,N-1 \tag{3.29}$$

where $\varepsilon(m)$ is the partial energy of the minimum delay sequence

and $\varepsilon_i(m)$ is the partial energy of the ith sequence in the suite.

An interesting property of minimum phase systems is that their impulse response is a minimum delay sequence. For example, consider a minimum phase system with z-transform $H(z)$ where

$$H(z) = Q(z)(1 - z_0 z^{-1}), \quad |z_0| < 1 \tag{3.30}$$

where $Q(z)$ is the z-transform of another minimum phase system

and z_0 is a zero of $H(z)$.

Let $H_1(z)$ be the z-transform of a non-minimum phase system that has a zero at $z = 1/z_0^*$ instead of at $z = z_0$, i.e.,

$$H_1(z) = Q(z)(z^{-1} - z_0^*) \tag{3.31}$$

The corresponding impulse responses are:

$$h(n) = q(n) * \left[\delta(n) - z_0 \delta(n-1)\right] \tag{3.32}$$

and

$$h_1(n) = q(n) * \left[-z_0^* \delta(n) + \delta(n-1)\right] \tag{3.33}$$

where $q(n)$ is the IDFT of $Q(z)$. Consider their partial energies $\varepsilon(m)$ and $\varepsilon_1(m)$, where

$$\begin{aligned}\varepsilon(m) &= \sum_{n=0}^{m} |h(n)|^2 \\ &= \sum_{n=0}^{m} |q(n)|^2 - z_0^* \sum_{n=0}^{m} q^*(n-1) q(n) - z_0 \sum_{n=0}^{m} q(n-1) q^*(n) + |z_0|^2 \sum_{n=0}^{m} |q(n-1)|^2\end{aligned} \tag{3.34}$$

and

$$\begin{aligned}\varepsilon_1(m) &= \sum_{n=0}^{m} |h_1(n)|^2 \\ &= |z_0|^2 \sum_{n=0}^{m} |q(n)|^2 - z_0^* \sum_{n=0}^{m} q^*(n-1) q(n) - z_0 \sum_{n=0}^{m} q(n-1) q^*(n) + \sum_{n=0}^{m} |q(n-1)|^2\end{aligned} \tag{3.35}$$

The difference in their partial energies is

$$\begin{aligned}\varepsilon(m) - \varepsilon_1(m) &= \left(1 - |z_0|^2\right) \sum_{n=0}^{m} |q(n)|^2 + \left(|z_0|^2 - 1\right) \sum_{n=0}^{m} |q(n-1)|^2 \\ &= \left(1 - |z_0|^2\right) |q(m)|^2 \\ &\geq 0\end{aligned} \tag{3.36}$$

since $|z_0| < 1$ and $|q(m)|^2 \geq 0$. Hence,

$$\varepsilon(m) \geq \varepsilon_1(m), \quad m = 0,1,\ldots,N-1 \tag{3.37}$$

or equivalently, the impulse response of a minimum phase system is a minimum delay sequence. Similarly, it can be shown that the impulse response of a maximum phase system is a *maximum delay sequence*, i.e., a sequence for which

$$\varepsilon(m) \leq \varepsilon_i(m), \quad i = 0,1,\ldots,2^{N-1}-1; \; m = 0,1,\ldots,N-1 \tag{3.38}$$

3.4.2 The RMS Delay Spread of a Minimum Phase Channel

A channel's RMS delay spread is a function of its impulse response. If the channel is minimum phase it is possible to determine the transfer function, accurate to within a linear phase shift and denoted as $\tilde{H}(e^{j\omega})$, with knowledge of $|H(e^{j\omega})|$ only. The corresponding impulse response $\tilde{h}(n)$ is calculated via the IDFT of $\tilde{H}(e^{j\omega})$ and is accurate to within a constant time shift.

A constant time shift does not change the difference between the arrival time of the nth path and the arrival time of the first path [see Equations (3.2) and (3.3)], nor does it change the envelope of the nth path relative to the first path. Hence τ_{rms} may be calculated using $\tilde{h}(n)$.

Consider $H(z)$ in polar form, i.e.,

$$H(z) = |H(z)| e^{j \arg[H(z)]} \tag{3.39}$$

The complex natural logarithm of $H(z)$ is [Oppenheim and Schafer, pp. 345-346]

$$\hat{H}(z) = \ln[H(z)] = \ln|H(z)| + j \arg[H(z)] \tag{3.40}$$

If $\hat{H}(z)$ is the *z*-transform of $\hat{h}(n)$, Equation (3.18) implies that

$$\arg[H(e^{j\omega})] = \Psi\left[\ln\left|H(e^{j\omega})\right|\right] \tag{3.41}$$

if and only if $\hat{h}(n)$ is causal and stable. Furthermore, $\ln|H(z)|$ diverges when $H(z)=0$ so $H(z)$ cannot contain zeros (or poles) in its region of convergence. Hence $\hat{h}(n)$ is causal and stable if and only if $H(z)$ is minimum phase.

Upon closer inspection of Equation (3.41), however, it is evident that $\arg[H(e^{j\omega})]$ is accurate only to within a linear phase shift. To illustrate this point, consider two minimum phase systems with transfer functions $G_1(e^{j\omega})$ and $G_2(e^{j\omega})$. Suppose that

$$g_1(n) > 0, \quad n = 0 \tag{3.42}$$

and

$$g_2(n) = g_1(n - n_0), \quad n_0 > 0 \tag{3.43}$$

Then

$$G_2\left(e^{j\omega}\right) = e^{-j\omega n_0} G_1\left(e^{j\omega}\right) \tag{3.44}$$

Since both systems are causal,

$$\begin{aligned} g_1(n) &= 0, \quad n < 0 \\ g_2(n) &= 0, \quad n < n_0 \end{aligned} \tag{3.45}$$

Equation (3.41) suggests that

$$\arg[G_1(e^{j\omega})] = \Psi\left[\ln\left|G_1(e^{j\omega})\right|\right] \tag{3.46}$$

and

$$\arg[G_2(e^{j\omega})] = \Psi\left[\ln\left|G_2(e^{j\omega})\right|\right] \tag{3.47}$$

However, since

$$\left|G_2(e^{j\omega})\right| = \left|G_1(e^{j\omega})\right| \tag{3.48}$$

the linear phase shift of $-\omega n_0$ in $G_2(e^{j\omega})$ is lost [Equation (3.47)]. Hence, Equation (3.41) is completely correct if and only if $H(e^{j\omega})$ has zero phase shift. Equation (3.41) is corrected by simply adding a term to account for a linear phase shift of $-\omega n_0$, i.e.,

$$\arg[H(e^{j\omega})] = \Psi\left[\ln\left|H(e^{j\omega})\right|\right] - \omega n_0 \tag{3.49}$$

where, for completeness,

$$\begin{aligned} h(n-n_0) > 0, &\quad n = n_0 \\ h(n-n_0) = 0, &\quad n < n_0 \end{aligned} \tag{3.50}$$

Since a constant time shift in the impulse response does not affect τ_{rms}, Equation (3.41) may be used in its calculation provided, of course, that the channel is minimum phase; specifically,

$$\tilde{H}\left(e^{j\omega}\right) = \left|H\left(e^{j\omega}\right)\right| e^{j\Psi\left[\ln\left|H\left(e^{j\omega}\right)\right|\right]} \tag{3.51}$$

τ_{rms} is calculated by using $\tilde{h}(n)$ [i.e., the IDFT of $\tilde{H}(e^{j\omega})$] in Equations (3.2) and (3.3) with a set to zero.

CHAPTER FOUR

System Causality

A physically realizable system operating in real time must be causal. Hence, in order to assert the validity of the frequency domain measurement system, it is prudent to examine the (measured) transfer function of the experimental channel *vis à vis* causality. The results of this chapter form the basis of the investigation into the minimum phase properties of the experimental channel (Chapter Five).

4.1 Statistical Curve Comparisons

It was shown in Section 3.3 that the imaginary part of a system's transfer function is the Hilbert transform of the real part of its transfer function if and only if the system is causal. Since both $H_I(e^{j\omega})$ and $H_R(e^{j\omega})$ are experimentally available, it is possible to statistically compare $H_I(e^{j\omega})$ and $\Psi[H_R(e^{j\omega})]$. A straightforward method is to consider the correlation between the curves $H_I(e^{j\omega})$ versus ω and $\Psi[H_R(e^{j\omega})]$ versus ω, and the difference in their means. If the curves are highly correlated and their means are not significantly different, then $\{\Psi[H_R(e^{j\omega})]\}$ is a good estimate of $\{H_I(e^{j\omega})\}$, i.e., the channel is causal.

The *linear correlation coefficient*, often denoted simply as *r*, is a value between -1 and 1 that indicates the degree of linear correlation between two equally sized data sets $\{x\}$ and $\{y\}$. When $|r|$ is close to unity a high degree of correlation exists; when $|r|$ is close to zero the data sets are uncorrelated. The square of the correlation coefficient, the *coefficient of determination*, is the proportion of the total variation of $\{y\}$ which is accounted for by its relationship with $\{x\}$ [Freund and Walpole, pg. 443]. For example, an r value of 0.90 indicates that 81% of the variation of $\{y\}$ is accounted for by its relationship with $\{x\}$.

It is possible that $\{H_I(e^{j\omega})\}$ and $\{\Psi[H_R(e^{j\omega})]\}$ could be highly correlated (i.e., r^2 close to unity) but have significantly different means. In this situation $\{\Psi[H_R(e^{j\omega})]\}$ is not a good estimate of $\{H_I(e^{j\omega})\}$. The Student's t-test for significantly different means tests the null hypothesis that two data sets do not have significantly different means [Press *et al.*, pp. 482-485]. The *t-statistic* α_t is a number between zero and one that is used to accept or reject the null hypothesis. The null hypothesis is rejected with $(1-\alpha_t)100\%$ confidence. It is common to accept the null hypothesis unless it can be rejected with at least 95% confidence. Hence, it is assumed that two data sets have significantly different means if and only if $\alpha_t \leq 0.05$. The following sections use the coefficient of determination and the t-statistic in analysis of the channel's causality (i.e., the measurement system's validity).

4.2 Channel Causality Testing

Various measurements of the experimental channel's transfer function were used to analyze the channel's causality. For each data set, $\{\Psi[H_R(e^{j\omega})]\}$ was computed and the coefficient of determination and t-statistic of $\{H_I(e^{j\omega})\}$ and $\{\Psi[H_R(e^{j\omega})]\}$ were examined. The results for the distance-oriented measurements are presented in Subsection 4.2.1; the results for the frequency-oriented measurements are discussed in Subsection 4.2.2.

4.2.1 Causality for Distance-Oriented Measurements

The graph in Figure 4.1 shows α_t and r^2 for the distance-oriented data sets $\{H_I(e^{j\omega})\}$ and $\{\Psi[H_R(e^{j\omega})]\}$ centred at 1000 MHz with a bandwidth of 200 MHz. $\alpha_t > 0.05$ for antenna separations of approximately 4 m to 30 m; hence, the null hypothesis that the means of $\{H_I(e^{j\omega})\}$ and

$\{\Psi[H_R(e^{j\omega})]\}$ are not significantly different is accepted over this range. r^2 is extremely close to unity throughout the aforementioned range; this indicates a very high degree of correlation between $\{H_I(e^{j\omega})\}$ and $\{\Psi[H_R(e^{j\omega})]\}$. It is therefore concluded that the channel is causal for antenna separations of 4 m to 30 m and a frequency centre of 1000 MHz.

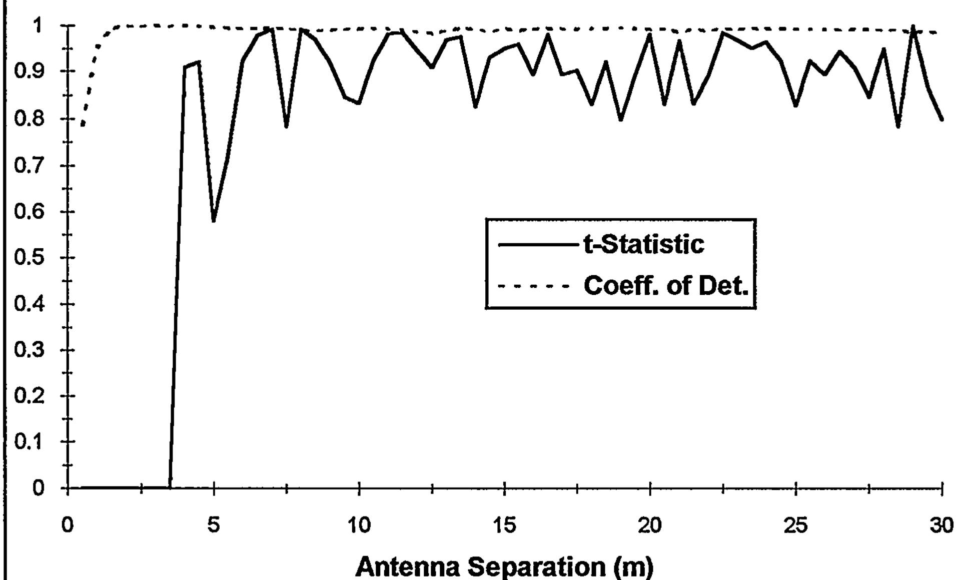

Fig. 4.1: 1000 MHz Distance-Oriented Data Set Comparison

To explain the apparent non-causality of the channel for antenna separations less than 4 m, consider the impulse response of the channel for an antenna separation of 0.5 m (Figure 4.2). The reason for the apparent non-causality is made clear in this graph - a significant portion of the first arrival is in negative time. This apparent physical impossibility is explainable upon investigation of the impulse response calculation. The impulse response was not measured, rather, it was calculated via the IDFT of the transfer function $H(e^{j\omega})$. Recall (Subsection 2.3.2) that it is necessary to window $H(e^{j\omega})$ before taking the IDFT. The window is applied to $H(e^{j\omega})$ via a multiplication; this is equivalent to a time domain convolution with $h(n)$, which smears the impulse response. The impulse response is smeared across the resolving bandwidth of the Blackman-Harris leakage function - approximately 2.3 bins (see Figure 2.6). Since the bandwidth of the impulse response is 200 MHz, the time domain bin resolution is $2.3 \cdot (1/200\,\text{MHz}) = 11.5\,\text{ns}$. Hence, when the transmit and receive antennas are separated by less than 3.45 m, some of the first arrival will be smeared into negative time. Figure 4.3 shows the impulse response for an antenna separation of 15 m. The precursor that appears at approximately -200 ns is explained below.

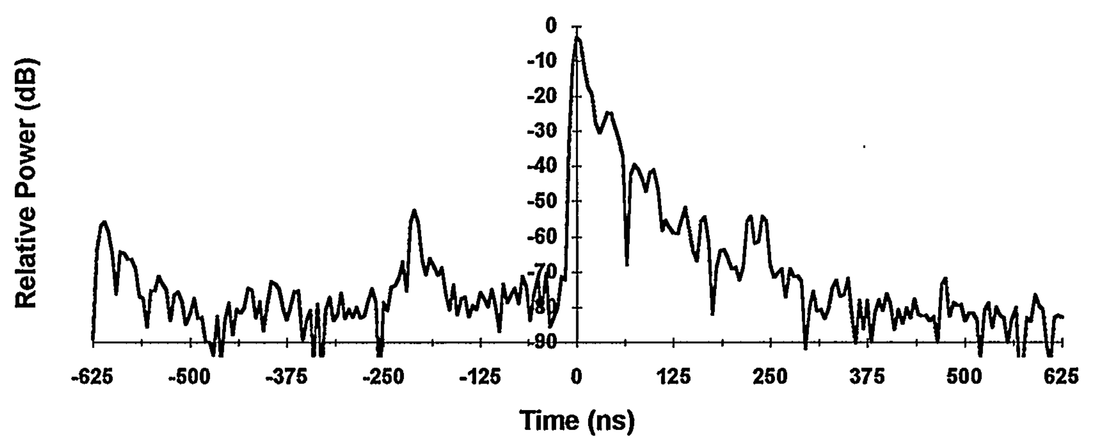

Fig. 4.2: 1000 MHz Impulse Response for 0.5 m Antenna Separation

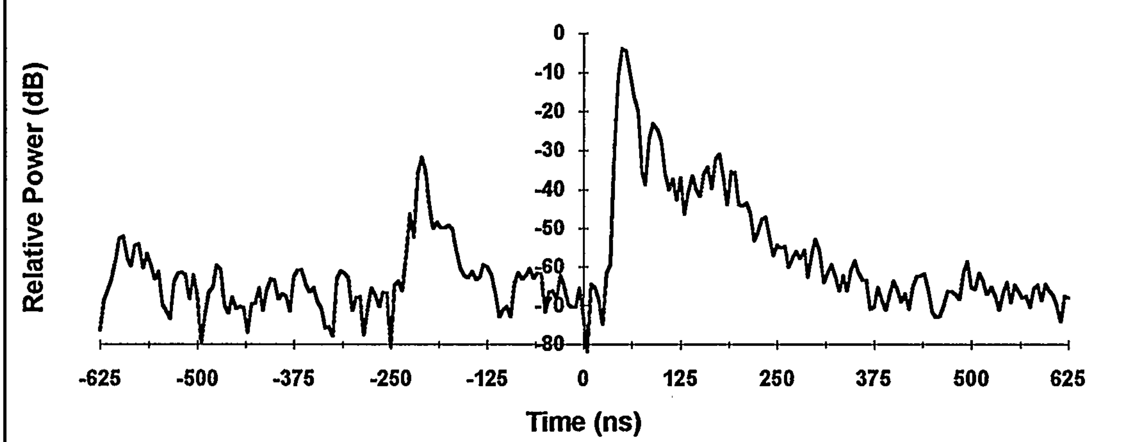

Fig. 4.3: 1000 MHz Impulse Response for 15 m Antenna Separation

The graph in Figure 4.4 shows α_t and r^2 for the distance-oriented data sets centred at 1600 MHz with a bandwidth of 200 MHz. The results for the 1600 MHz case are similar to those for the 1000 MHz case in that the channel appears causal for antenna separations of approximately 4 m to 30 m. However, there is clearly less correlation between $\{H_I(e^{j\omega})\}$ and $\{\Psi[H_R(e^{j\omega})]\}$ over this interval. The reason for the 1600 MHz channel appearing "less causal" than the 1000 MHz channel is due to the precursor at $t \approx -200$ ns. Figures 4.3 and 4.5 illustrate this phenomenon. In the 1000 MHz case, the relative power of the precursor is 28 dB less than that of the first arrival. The precursor is almost small enough to blend in with the noise and hence does not significantly alter the causality of the channel. In the 1600 MHz case, however, the precursor is only 8 dB below the relative power of the first arrival and contributes significantly to the overall power of the impulse response. This makes the 1600 MHz channel appear to be less causal than the 1000 MHz channel.

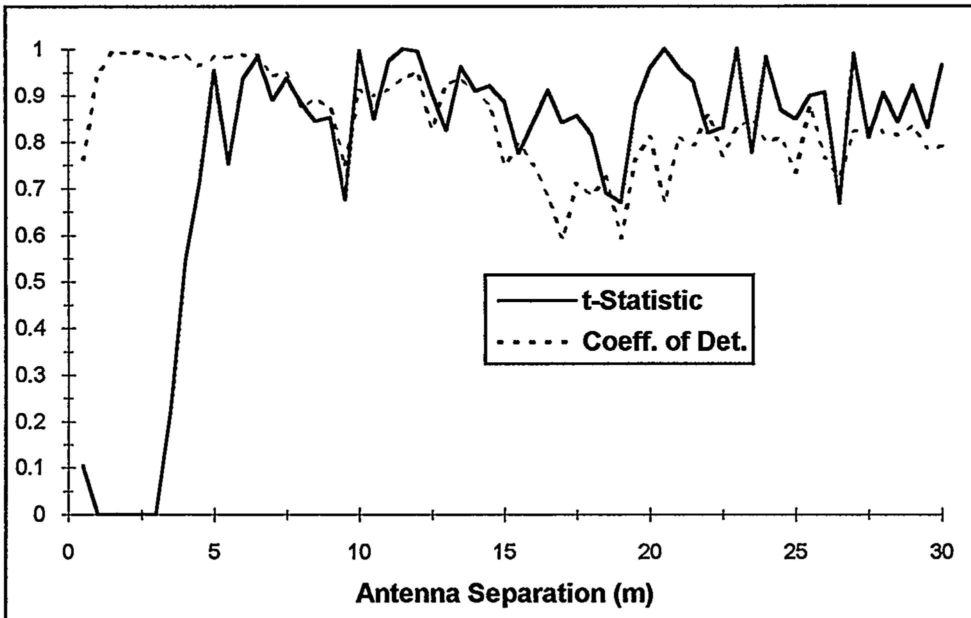

Fig. 4.4: 1600 MHz Distance-Oriented Data Set Comparison

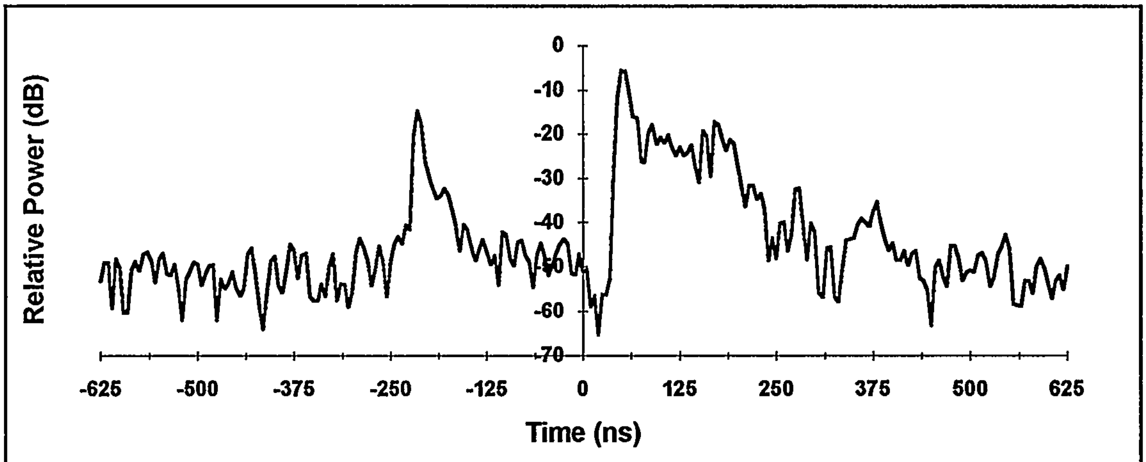

Fig. 4.5: 1600 MHz Impulse Response for 15 m Antenna Separation

The precursor is a result of crosstalk between the transmit and receive cables; it is not a multipath component that has been aliased into negative time due to the periodic nature of the IDFT. The network analyzer is calibrated to measure the time it takes the test signal to travel from the transmit antenna to the receive antenna, hence the time it takes for the signal to travel through the cables is not included. When crosstalk occurs close to the transmit and receive terminals, the received signal (due to the crosstalk) will appear to arrive in negative time. Since the total cable length is 57.8 m (see Figure 2.1), the precursor will occur at approximately -193 ns. To verify the assumption of crosstalk, the frequency domain sampling rate was doubled to extend the time domain response from -1250 ns to +1250 ns. If the precursor had been a result of an aliased multipath component it would have appeared at approximately 1050 ns in the over sampled impulse response. However, the precursor still appeared at approximately –200 ns. The crosstalk is more prevalent at 1600 MHz than at 1000 MHz, which gives rise to a larger precursor at 1600 MHz.

4.2.2 Causality for Frequency-Oriented Measurements

Figure 4.6 shows α_t and r^2 averaged over the data sets corresponding to an 11 m to 12 m LOS antenna separation, a centre of frequency sweep from 1080 MHz to 2420 MHz, and a bandwidth of 160 MHz. The results displayed in Figure 4.6 indicate that the channel is indeed causal over the aforementioned range. The data sets $\{H_I(e^{j\omega})\}$ and $\{\Psi[H_R(e^{j\omega})]\}$ are highly correlated $(r^2 \approx 1)$, however, the assertion that their means do not significantly differ is weaker than for the distance-oriented data sets. But α_t is still well within the 95% confidence interval and therefore the null hypothesis that their means are not significantly different is accepted.

Figure 4.7 shows α_t and r^2 averaged as described above, but for a NLOS antenna separation. The results are consistent with α_t and r^2 for the LOS data. This indicates that the causality of the indoor channel is not related to the sight line of the antennas.

For completeness, sample impulse responses for the LOS and NLOS cases are shown in Figures 4.8 and 4.9, respectively. In both graphs the antenna separation is 12 m and the frequency centre is 1680 MHz. It is of interest to note that the first arrival in the NLOS case is not the strongest.

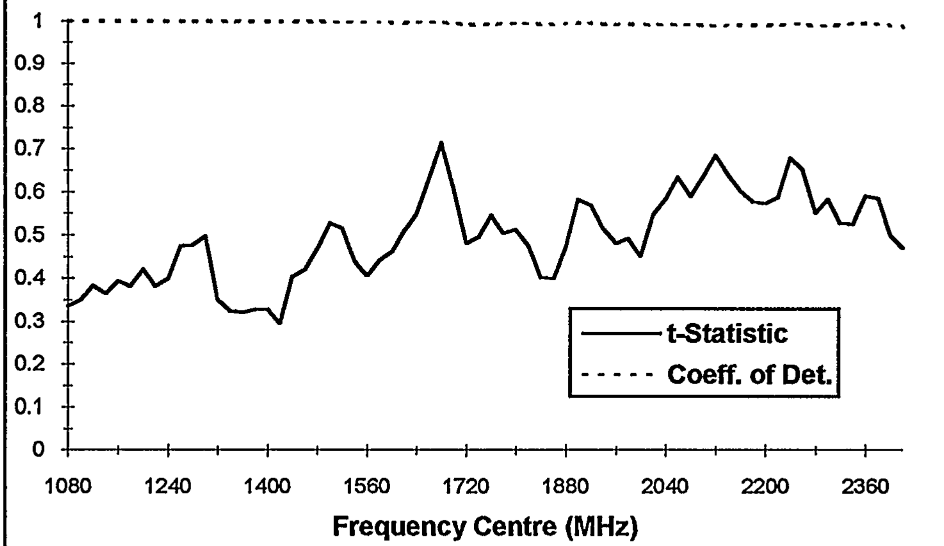

Fig. 4.6: LOS Frequency-Oriented Data Set Comparison Averaged Over 11 m to 12 m Antenna Separation

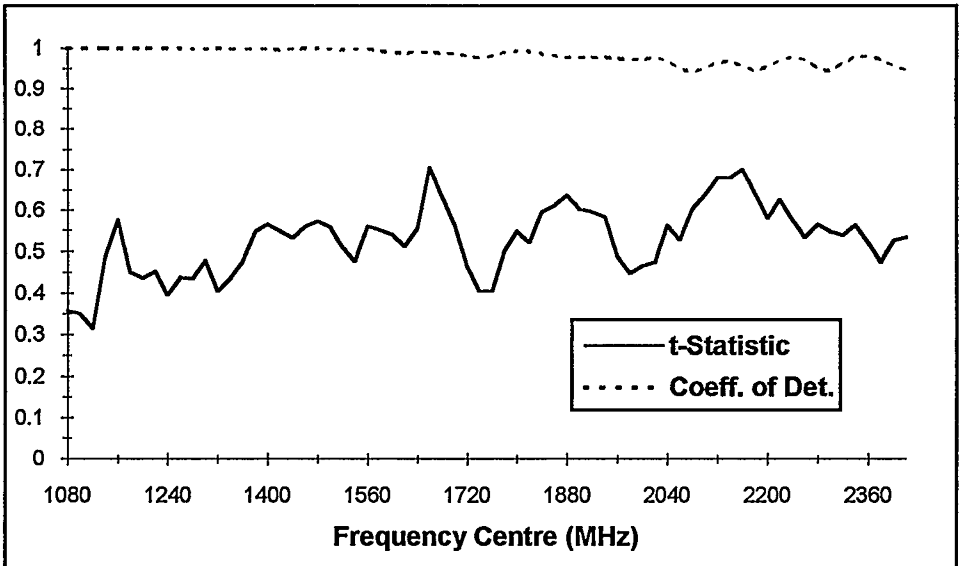

Fig. 4.7: NLOS Frequency-Oriented Data Set Comparison Averaged Over 11 m to 12 m Antenna Separation

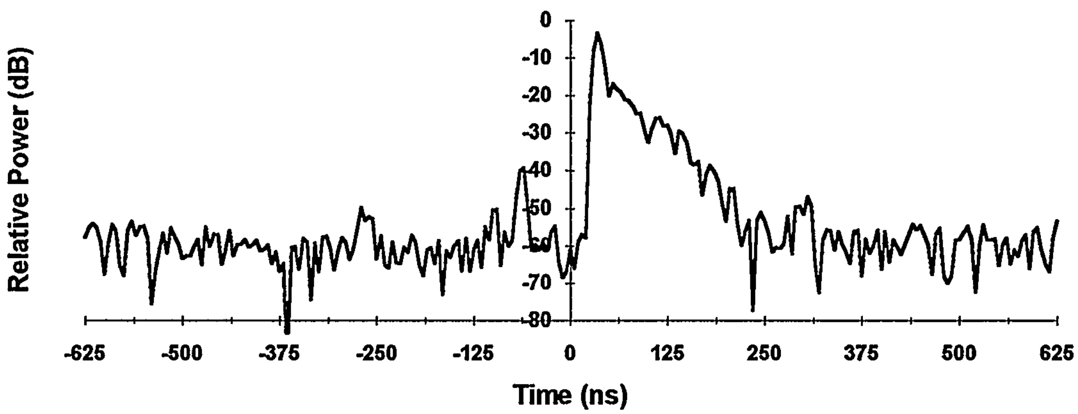

Fig. 4.8: 1680 MHz LOS Impulse Response for 12 m Antenna Separation

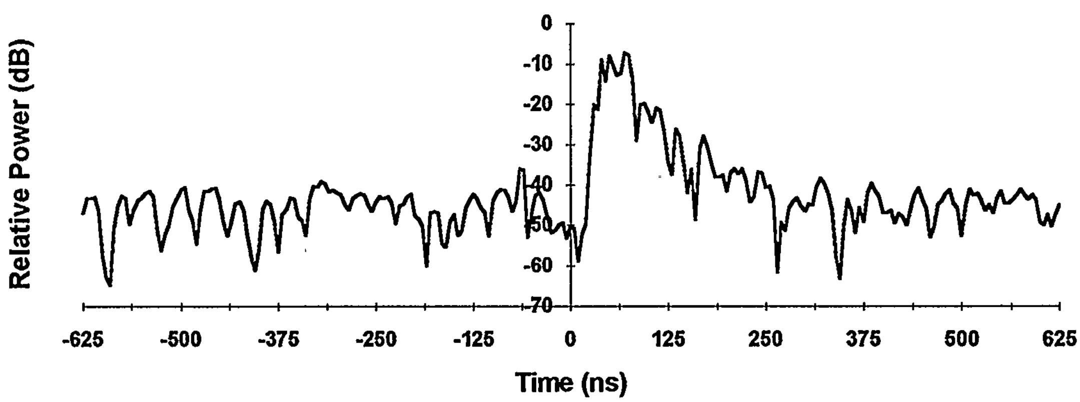

Fig. 4.9: 1680 MHz NLOS Impulse Response for 12 m Antenna Separation

CHAPTER FIVE

Channel Characterization Analysis

The results of the experimental channel's characterization are presented and analyzed in this chapter. Section 5.1 explores the difference between the channel's true RMS delay spread and the estimations made under minimum phase assumptions. Section 5.2 introduces environmental influences that make τ_{rms} frequency dependent.

5.1 Analysis of the RMS Delay Spread

If a system is causal, the imaginary part of its transfer function is the Hilbert transform of the real part of its transfer function (Section 3.3). Furthermore, if the system is minimum phase it is possible to determine the phase of its transfer function (with linear phase shift ambiguity) with knowledge of its magnitude spectrum only (Subsection 3.4.2). The impulse response (with constant time shift ambiguity) can be calculated via the inverse Fourier transform.

Under the assumption of a minimum phase channel, the impulse response $\tilde{h}(n)$ was calculated using only the magnitude of the experimental channel's frequency response. Impulse response data were collected using the distance-oriented and frequency-oriented measurements described in Section 2.2. Using each data set, the true and estimated RMS delay spreads (τ_{rms} and $\tilde{\tau}_{rms}$, respectively) were calculated using the appropriate impulse response ($h(n)$ or $\tilde{h}(n)$, respectively). To aid in the explanation of the RMS delay spread results, the zeros of the channel's z-transform were calculated. As expected, there is a strong correlation between the percentage of zeros inside the unit circle and the difference between τ_{rms} and $\tilde{\tau}_{rms}$.

5.1.1 RMS Delay Spread Results for Distance-Oriented Measurements

Figure 5.1 shows plots of $h(n)$ and $\tilde{h}(n)$ for the distance-oriented data with an antenna separation of 15 m, a centre of frequency of 1000 MHz, and a bandwidth of 200 MHz. In the region of high SNR,

$$\tilde{h}(n-n_0) \approx h(n) \tag{5.1}$$

where n_0 is the first arrival of $h(n)$. Obviously, $\tilde{h}(n)$ is not a good estimate of $h(n)$ outside this region. Note that the precursor located at $t \approx -200$ ns (Subsection 4.2.1) is not present in $\tilde{h}(n)$ since the calculation of $\tilde{h}(n)$ assumes channel causality. Figure 5.2 shows $h(n)$ and $\tilde{h}(n-n_0)$ in the region of high SNR (assumed to be from n_0 to $n_0 + 200\,\text{ns}$). The results are excellent, indicating that the 1000 MHz channel (with an antenna separation of 15 m) is nearly minimum phase. Similar results were obtained for the 1000 MHz channel for antenna separations of 4 m to 30 m.

To eliminate the effects of noise, τ_{rms} was calculated using the impulse response $g(n)$, where

$$g(n) = \begin{cases} h(n), & n_0 \le n \le n_0 + 200\,\text{ns} \\ 0, & \text{elsewhere} \end{cases} \tag{5.2}$$

Similarly, $\tilde{\tau}_{rms}$ was calculated using $\tilde{g}(n)$, where

$$\tilde{g}(n) = \begin{cases} \tilde{h}(n), & 0 \le n \le 200\,\text{ns} \\ 0, & \text{elsewhere} \end{cases} \tag{5.3}$$

Figure 5.3 shows τ_{rms} and $\tilde{\tau}_{rms}$ versus antenna separation for the 1000 MHz channel. At each measurement the percentage of zeros inside the unit circle is shown. To calculate the location of the zeros, the members of $\{h(n)\}$ were used as z-transform coefficients in the region of high SNR. The location of the zeros demonstrates that the channel is nearly minimum phase. The reason that the 1000 MHz channel is not entirely minimum phase is likely due to the slight non-causality caused by the precursor.

Figures 5.4 and 5.5 show $h(n)$ and its corresponding estimate for an antenna separation of 15 m, a centre of frequency of 1600 MHz, and a bandwidth of 200 MHz. Similar results were obtained for antenna separations of 4 m to 30 m. $\tilde{h}(n)$ for the 1600 MHz channel is a poorer estimate of $h(n)$ than is $\tilde{h}(n)$ for the 1000 MHz channel. This is likely due to the much larger precursor present in the 1600 MHz data. Slightly poorer results are also evident in the comparison of τ_{rms} and $\tilde{\tau}_{rms}$ versus distance (Figure 5.6). This channel appears not as close to minimum phase as the 1000 MHz channel.

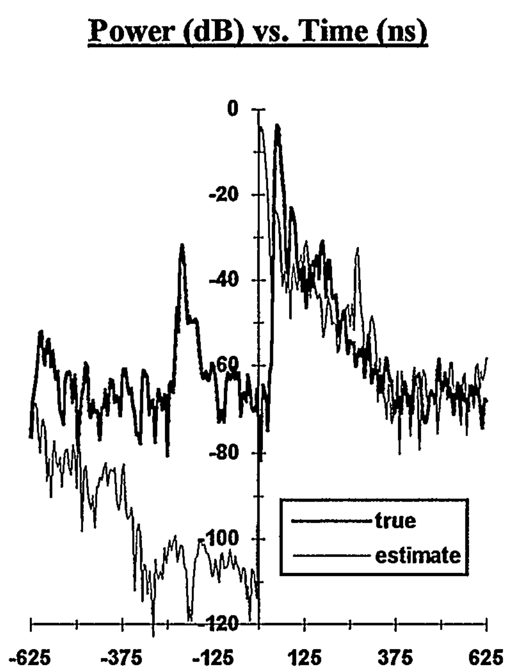

Fig. 5.1: 1000 MHz Impulse Responses for 15 m Antenna Separation

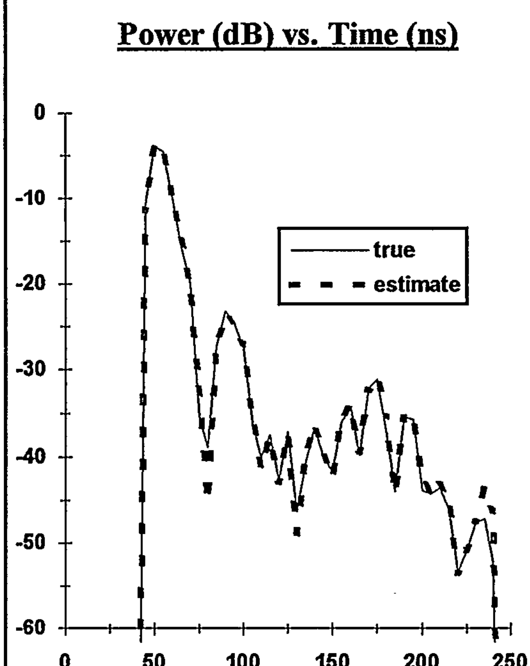

Fig. 5.2: 1000 MHz Impulse Responses for 15 m Antenna Separation

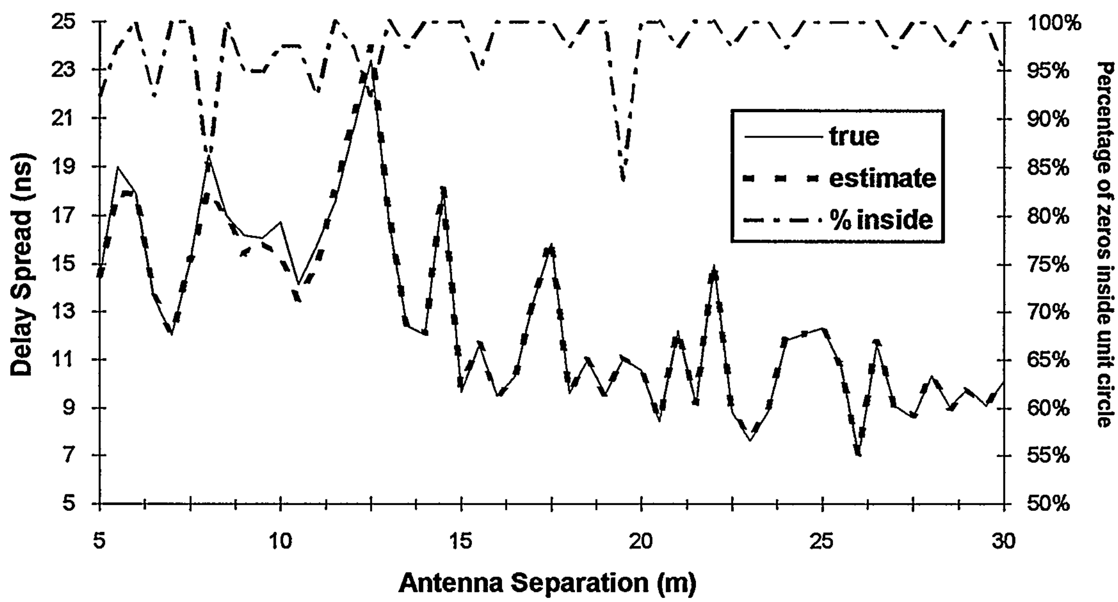

Fig. 5.3: 1000 MHz RMS Delay Spread and Minimum Phase Properties

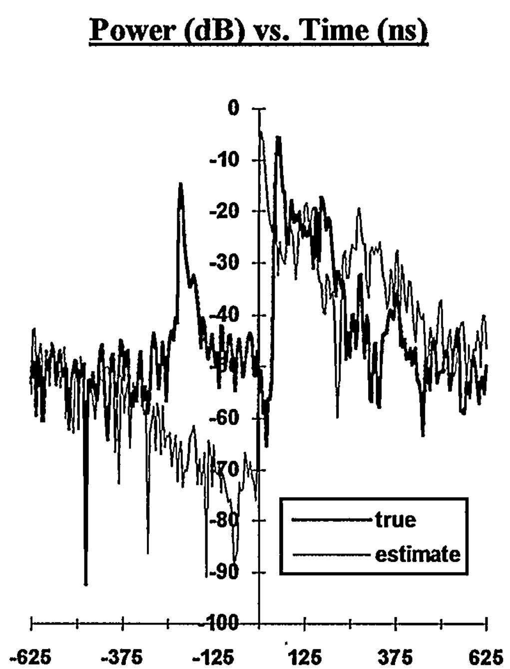

Fig. 5.4: 1600 MHz Impulse Responses for 15 m Antenna Separation

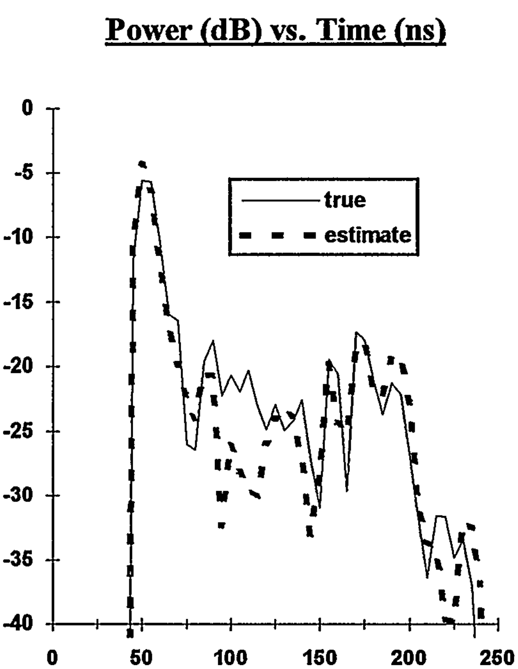

Fig. 5.5: 1600 MHz Impulse Responses for 15 m Antenna Separation

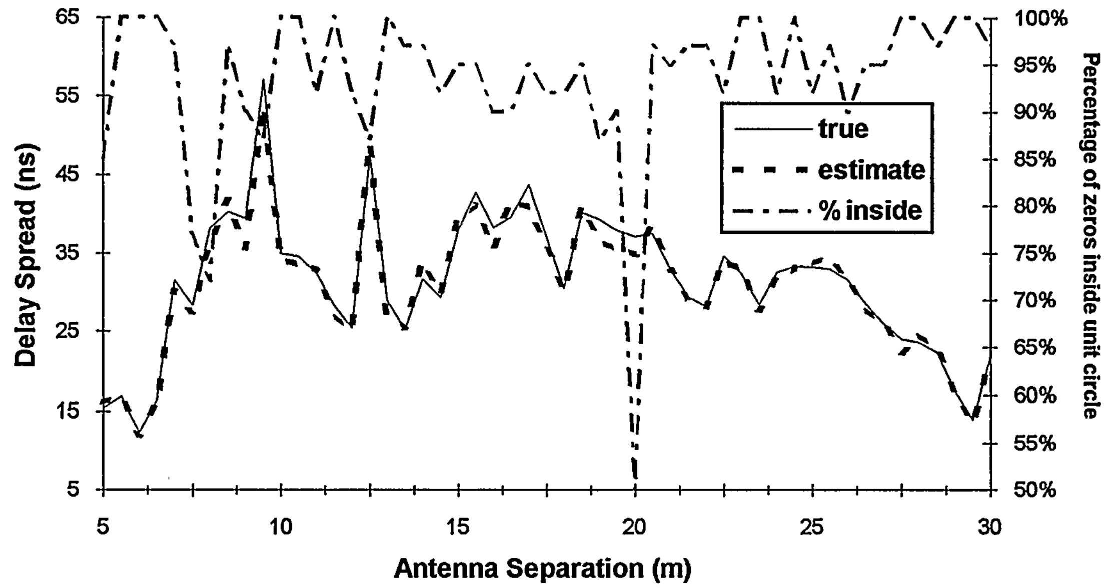

Fig. 5.6: 1600 MHz RMS Delay Spread and Minimum Phase Properties

5.1.2 RMS Delay Spread Results for Frequency-Oriented Measurements

Figure 5.7 shows $h(n)$ and $\tilde{h}(n)$ for a 160 MHz bandwidth LOS sample centred at 1680 MHz with an antenna separation of 12 m. The high SNR regions of $h(n)$ and $\tilde{h}(n-n_0)$ are compared in Figure 5.8. The results indicate that the 1680 MHz channel is nearly minimum phase, although it's not as close to minimum phase as, say, the 1000 MHz distance-oriented channel. The results of the comparisons of $h(n)$ and $\tilde{h}(n-n_0)$ are not similar across all frequency centres from 1080 MHz to 2420 MHz. For example, $h(n)$ and $\tilde{h}(n-n_0)$ are almost identical at 1420 MHz (Figure 5.10) but not at 1680 MHz (Figure 5.8). The apparent discrepancy in results between the 1680 MHz channel and the 1420 MHz channel can be attributed to an environmental influence present at 1680 MHz but not at 1420 MHz. This influence alters $h(n)$ at 1680 MHz to make the 1680 MHz channel less minimum phase than its 1420 MHz counterpart. This phenomenon is described in Section 5.2. Note that there is not an anti-causal influence (such as a large precursor) that is present in $h(n)$ at 1680 MHz but not at 1420 MHz (Figures

5.7 and 5.9). Hence, the discrepancy between the 1680 MHz and 1420 MHz channels can only be attributed to a difference in minimum phase properties - not in a significant difference in causality. Figure 5.11 shows τ_{rms} and $\tilde{\tau}_{\text{rms}}$ versus frequency for the LOS channel averaged over antenna separations of 11 m to 12 m. A decrease in the percentage of zeros inside the unit circle seems to result in an increase in τ_{rms}.

Figure 5.12 shows $h(n)$ and $\tilde{h}(n)$ for a 160 MHz bandwidth NLOS sample centred at 1680 MHz with an antenna separation of 12 m. Figure 5.13 shows the corresponding $h(n)$ and $\tilde{h}(n-n_0)$ in the region of high SNR. There is a significant discrepancy between the percentage of zeros inside the unit circle for the LOS and NLOS channels (Figures 5.11 and 5.14). The discrepancy is due to the fact that the impulse response energy of the LOS channel is more concentrated at the first arrival than is the energy of the NLOS channel. Recall that a channel is closer to minimum phase when the energy of $h(n)$ is concentrated at $n = n_0$ (Subsection 3.4.1). The fact that the NLOS channel is less minimum phase than the LOS channel is reflected in the poorer estimate of its RMS delay spread.

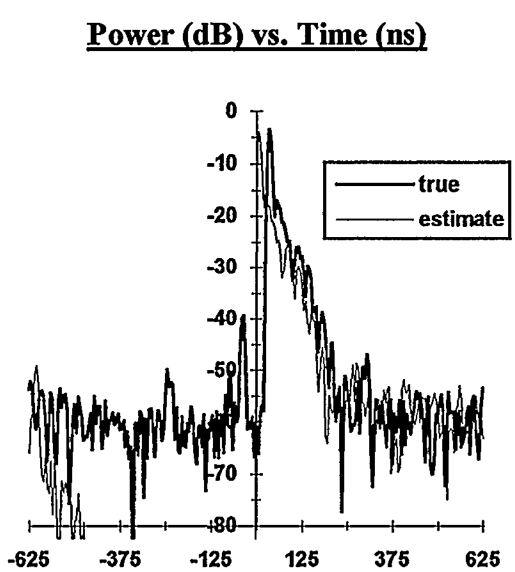

Fig. 5.7: 1680 MHz Impulse Responses for 12 m LOS Antenna Separation

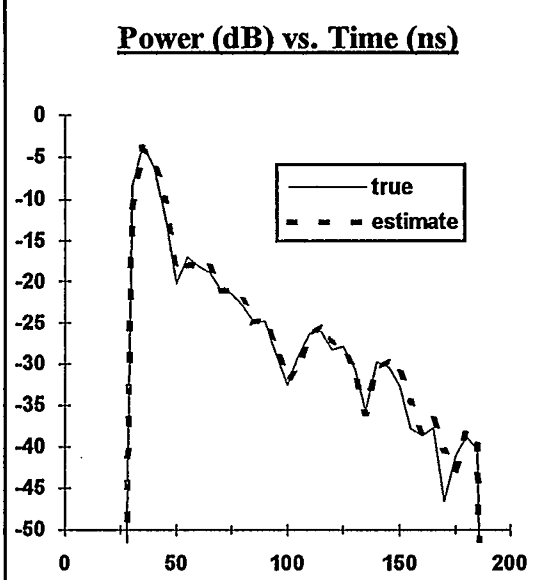

Fig. 5.8: 1680 MHz Impulse Responses for 12 m LOS Antenna Separation

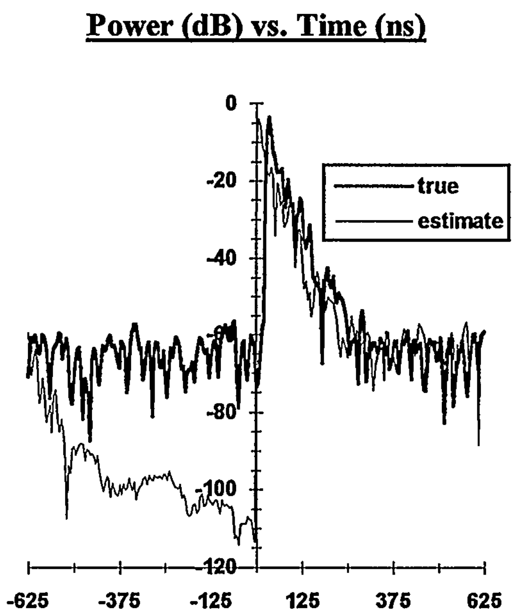

Fig. 5.9: 1420 MHz Impulse Responses for 12 m LOS Antenna Separation

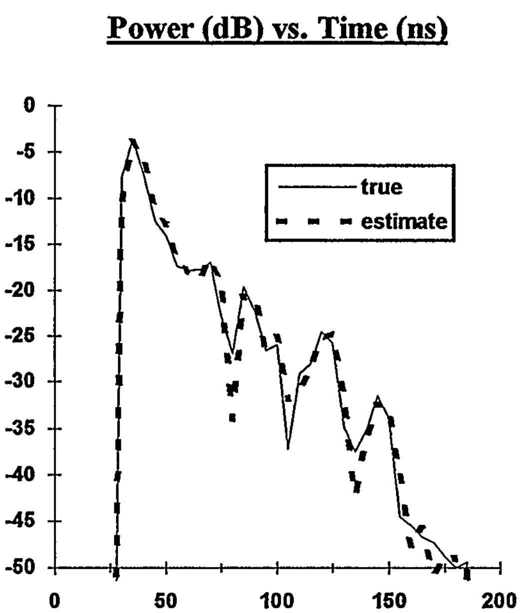

Fig. 5.10: 1420 MHz Impulse Responses for 12 m LOS Antenna Separation

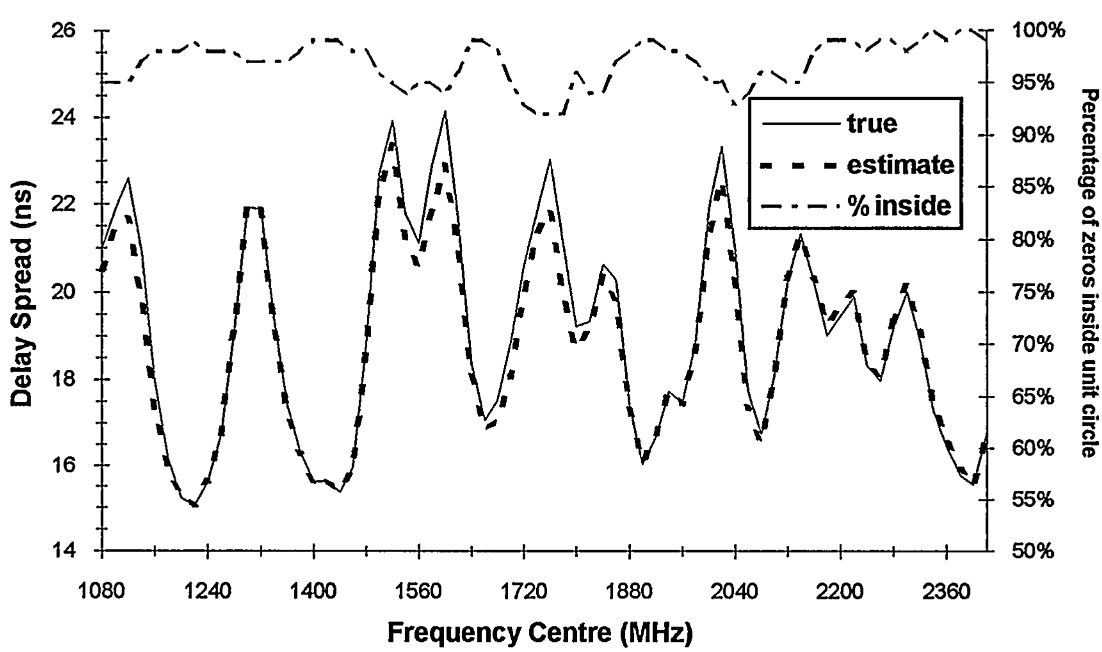

Fig. 5.11: LOS RMS Delay Spread and Minimum Phase Properties Averaged Over 11 m to 12 m

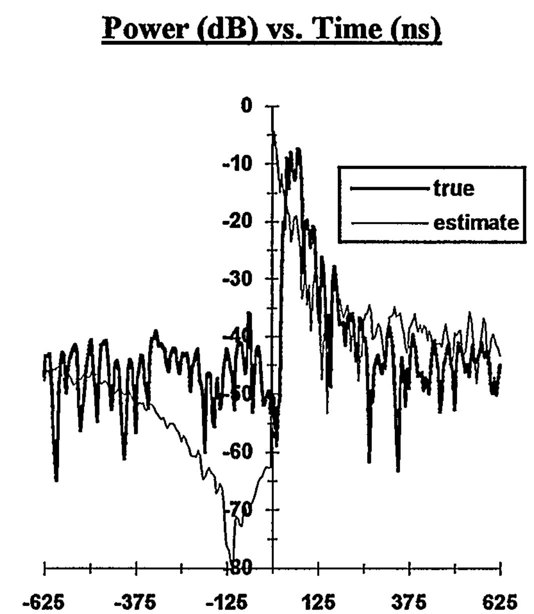

Fig. 5.12: 1680 MHz Impulse Responses for 12 m NLOS Antenna Separation

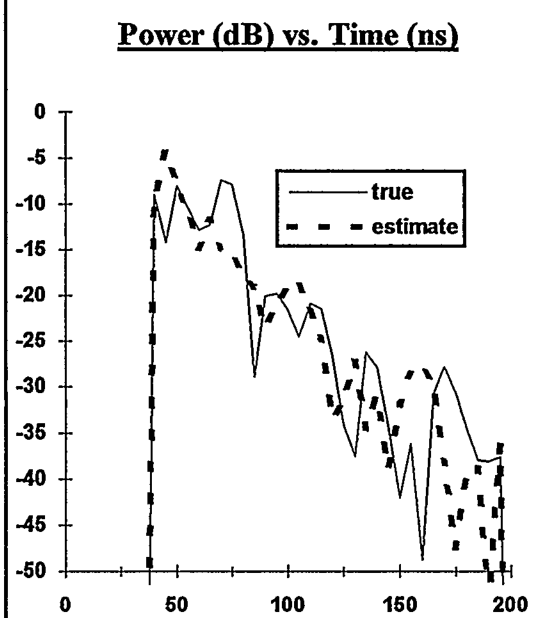

Fig. 5.13: 1680 MHz Impulse Responses for 12 m NLOS Antenna Separation

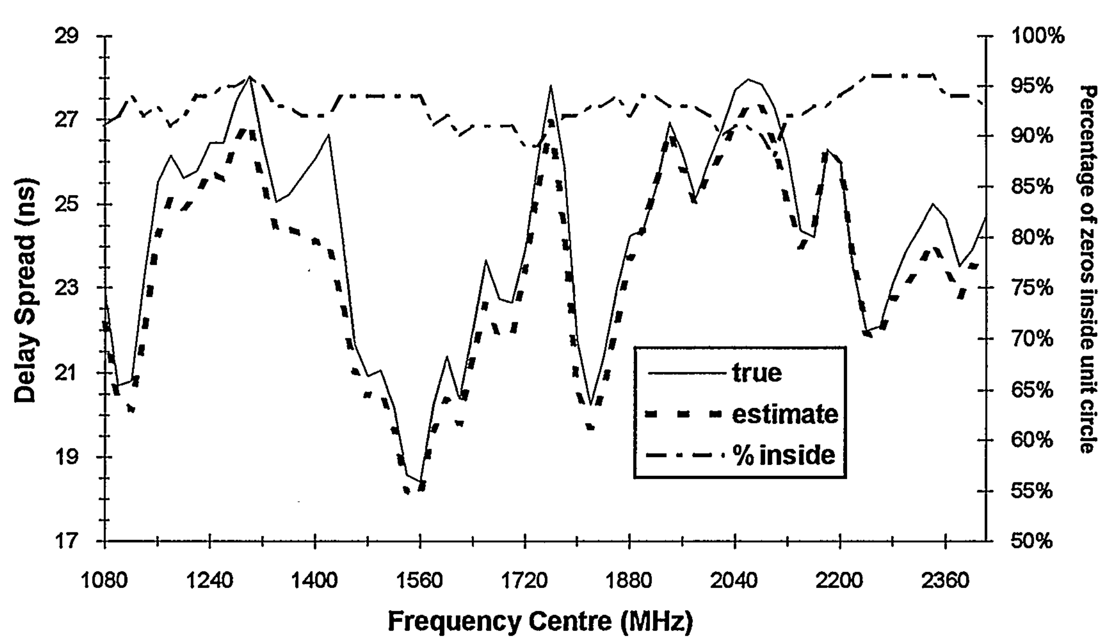

Fig. 5.14: NLOS RMS Delay Spread and Minimum Phase Properties Averaged Over 11 m to 12 m

5.2 Environmental Influences on Channel Characteristics

The data used for this thesis were collected entirely in the frequency domain. During each measurement channel stationarity was maintained, i.e., the channel did not physically change during a frequency sweep. Many researchers believe that the channel's multipath behavior does not change if the channel is stationary. This section gives an example of a stationary indoor communications channel (namely, the experimental channel used for the aforementioned data collection) whose multipath characteristics are dependent on the signaling frequency.

The explanation of the channel's frequency dependence requires an understanding of Fraunhofer diffraction and diffraction gratings. These subjects are typically associated with light waves and the study of optics, but the same principles also apply to electromagnetic (EM) waves. Given that the reader is likely somewhat familiar with diffraction *vis à vis* light waves and the study of optics, and that material on this subject is available in many undergraduate physics textbooks, the relevant concepts presented here are from the field of optics.

5.2.1 Fraunhofer Diffraction and Diffraction Gratings

Qualitatively speaking, diffraction is the flaring out of light as it emerges from the confines of a narrow slit. There are two general cases of diffraction: *Fresnel diffraction* and *Fraunhofer diffraction*.

Fresnel diffraction occurs when the light source and/or the screen on which the diffraction pattern is displayed are a finite distance away from the diffracting aperture. The light waves that enter and/or leave the aperture are not parallel. Figure 5.15 illustrates Fresnel diffraction [Halliday and Resnick, pg. 743].

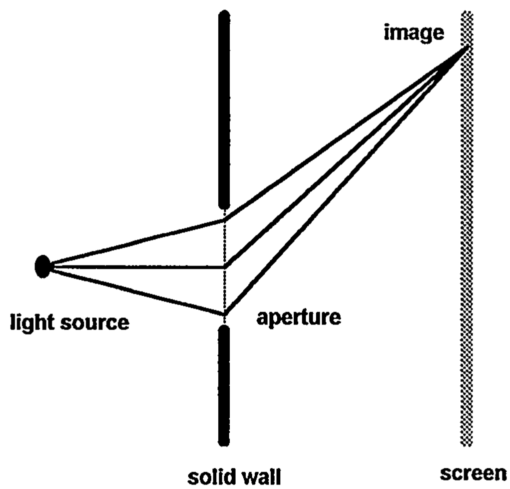

Fig. 5.15: Fresnel Diffraction

Souce and/or screen finite distance from aperture

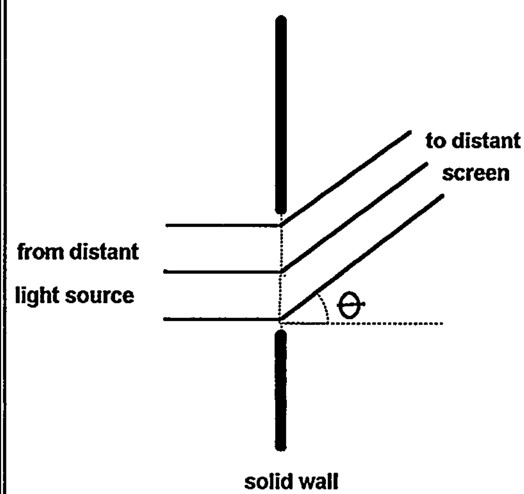

Fig. 5.16: Fraunhofer Diffraction

Souce and screen infinite distance from aperture

A special case of Fresnel diffraction, Fraunhofer diffraction, occurs when both the light source and screen are an infinite distance from the aperture. In this case the light waves entering and leaving the aperture are parallel. Fraunhofer diffraction is illustrated in Figure 5.16. The criterion for Fraunhofer diffraction is (see Figure 5.17) [Fowles. pg. 113]

$$\frac{1}{2}\left(\frac{1}{D_1}+\frac{1}{D_2}\right)\Delta^2 << \lambda \tag{5.4}$$

where D_1 is the horizontal distance from the source to the plane containing the aperture,

D_2 is the horizontal distance from the screen to the plane containing the aperture,

Δ is the width of the aperture,

and λ is the wavelength of the light.

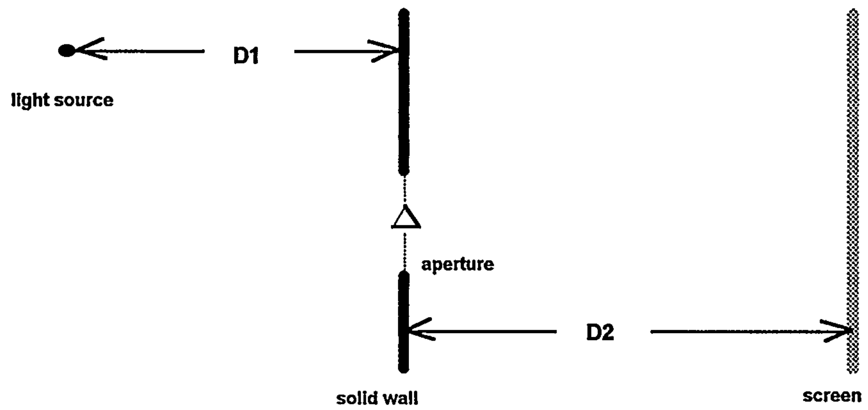

Fig. 5.17: Diffraction Parameters

If Equation (5.4) is not satisfied the diffraction is of the Fresnel type.

A multiple slit aperture is called a *diffraction grating*. A diffraction grating consisting of three identical apertures of width b and separation h is shown in Figure 5.18. For Fraunhofer diffraction, the light intensity I at point P is [Fowles, pp. 122-123]

$$I = I_0 \left(\frac{\sin \beta}{\beta} \right)^2 \left(\frac{\sin N\gamma}{N \sin \gamma} \right)^2 \tag{5.5}$$

where I_0 is the intensity for $\theta = 0$, i.e., no diffraction,

$\beta = \frac{\pi b}{\lambda} \sin \theta$,

$\gamma = \frac{\pi h}{\lambda} \sin \theta$,

and N is the number of apertures.

Equation (5.5) is used in Subsection 5.2.2 to show how the diffraction of EM waves can alter a stationary channel.

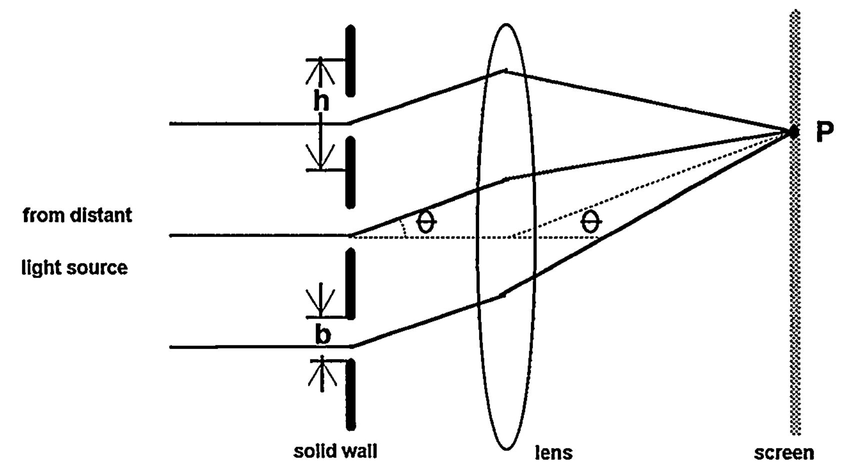

Fig. 5.18: Fraunhofer Diffraction via Diffraction Grating

5.2.2 Diffraction Gratings and the Experimental Channel

The experimental channel is described in Section 2.2. The solid wall (Figure 2.2) contains metal studs approximately two inches wide and sixteen inches apart. This wall acts as a diffraction grating for the EM waves. The antennas were approximately one metre from the wall; hence, over the frequency band used (1 GHz to 2.5 GHz) the diffraction is of the Fraunhofer type, i.e., Equation (5.4) is satisfied. The physical parameters are:

$$D_1 = D_2 = 1\,\text{m},$$

$$\Delta = 0.05\,\text{cm},$$

and $\lambda = c / f$

where $c = 3 \times 10^8\ \text{m/s}$

and $\quad 1\,\text{GHz} \le f \le 2.5\,\text{GHz}$.

Equation (5.4) is satisfied since $\frac{1}{2}\left(\frac{1}{1}+\frac{1}{1}\right)(0.05)^2 = 0.0025 << \min(\lambda) = 0.12$.

The Fraunhofer diffraction due to the diffraction grating is indeed significant in the experimental channel. Figure 5.19 plots the experimental channel's I/I_0 [Equation (5.5)] versus frequency for diffraction focused at the receiver. It is assumed that the hallway is 30 m long and that the transmitter is located in the centre (i.e., 15 m from either end of the hallway) which results in $N = 74$ apertures. Since the antennas are one metre from the wall, $\theta = 85°$ (see Figure 5.18) for a 12 m separation. The diffraction is very significant at 1480 MHz and 2220 MHz.

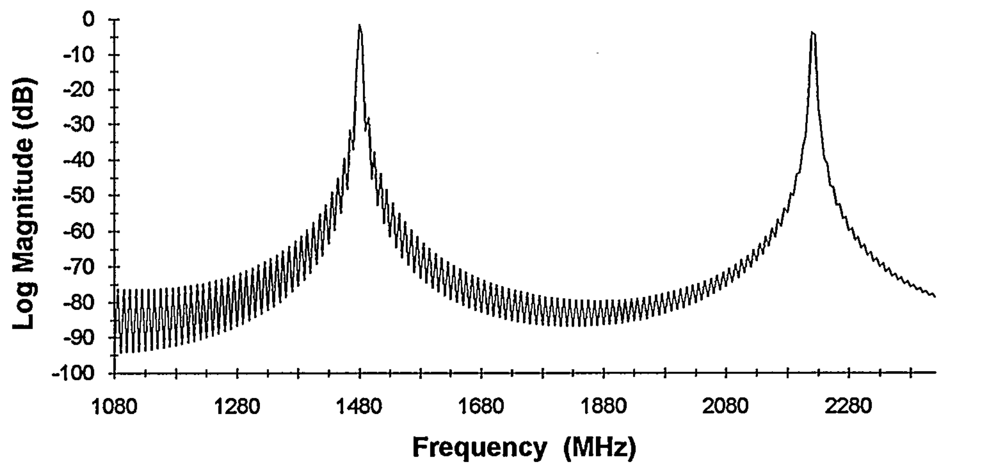

Fig. 5.19: I / Io vs. Frequency for 12 m Antenna Separation

In effect, a significant diffraction is a new multipath component. An extra multipath component may change the partial energy of a channel's impulse response. For example, if a channel is minimum phase without the extra multipath component, it may be non-minimum phase when the extra multipath component is present. A change in the channel's impulse response will likely result in a change in τ_{rms}.

The apparent frequency dependent behavior of τ_{rms} (see Figures 5.11 and 5.14) cannot be directly linked to the experimental channel's diffraction grating focused at the receiver. However, the diffraction grating is likely one environmental factor that contributes to the apparent frequency dependent nature of τ_{rms}. Many more such environmental factors may exist.

CHAPTER SIX

Conclusions

This thesis has examined wideband response parameters for the UHF indoor communications channel. The previous chapters have shown that some wideband parameters - specifically τ_{rms} - may be calculated with knowledge of the channel's frequency response magnitude spectrum only. Reasons for the apparent frequency dependency of τ_{rms} were also discussed.

6.1 Practical Use of the Results

To this author's knowledge, all frequency domain measurement systems in use today are similar to the one described in Chapter Two. This type of system has advantages over traditional time domain systems, such as the ability to perform both narrowband and wideband measurements and the improved temporal resolution of the impulse response [Morrison, pp. 100-102]. The potential disadvantages, however, are not insignificant. Because cables must run between both antennas and the network analyzer, the system is not practical to use unless both antennas are on the same floor of the building. This virtually precludes the system from being used to measure the outdoor channel or the outdoor-to-indoor channel. In addition, the network analyzer is an expensive piece of equipment that many RF research facilities do not have at their disposal; a network analyzer can cost up to $250,000. The results of this thesis suggest that a much cheaper and simpler alternate frequency domain measurement system exists. The alternate system enables the user to exploit the advantages of the frequency domain measurement systems (such as the improved temporal resolution), while eliminating some of the disadvantages.

It has been established that the phase spectrum of the indoor channel's frequency response need not be measured in order to obtain τ_{rms}. Therefore, τ_{rms} may be obtained via a device that measures the channel's frequency response magnitude spectrum only. A measurement system consisting of a spectrum analyzer and a signal generator would suffice. The use of a spectrum analyzer would eliminate the cable requirements as well as the high cost of a network analyzer. It is common for an RF lab to have a spectrum analyzer; they retail for approximately $15,000. A simple signal generator can be constructed with minimal effort and expense (several thousand dollars).

Few researchers have reported finding the frequency dependent nature of τ_{rms}; none have attempted to explain it. It was shown in Chapter Five that the diffraction grating created by metal studs in a wall may contribute to the frequency dependent nature of τ_{rms}. This frequency dependency cannot be entirely attributed to reflections caused by the diffraction grating; the diffraction grating may only be the tip of the iceberg in an environment full of frequency dependent reflectors. The results contained in this thesis show only that the indoor channel is frequency dependent.

6.2 Further Research

Many questions about the indoor communications channel remain unanswered and demand further research. Some of these topics have been highlighted in this thesis.

The fact that the indoor channel appears to be very close to minimum phase is no doubt a surprise to many researchers. This result should be verified by repeating the experiment in many different types of buildings. It would be useful to see if the (near) minimum phase property holds for large antenna separations or for channels that span more than one floor of the building. Data should be collected for the outdoor and outdoor-to-indoor channels to see if the outdoor channel exhibits minimum phase behavior.

No attempt was made in this thesis to justify the apparent dependency of τ_{rms} on antenna separation. Some researchers have reported observing such a dependency, while others have not (Section 1.1). Complete channel characterization requires the understanding of and ability to measure the frequency and path length dependent nature of τ_{rms}. This area requires further research.

REFERENCES

Bultitude, R. J. C., "Measurement, Characterization, and Modeling of Indoor 800/900 MHz Radio Channels for Digital Communications", *IEEE Communications Magazine*, Vol. 25, No. 6, June 1987, pp. 5-12.

Devasirvatham, D. M. J., "Time Delay Measurements of Wideband Radio Signals within a Building", *Electronic Letters*, Vol. 20, No. 23, 1984, pp. 950-951.

Devasirvatham, D. M. J., "Time Delay Spread and Signal Level Measurements of 850 MHz Radio Waves in Building Environments", *IEEE Transactions on Antennas and Propagation*, Vol. 34, No. 11, November 1986, pp. 1300-1305.

Fowles, G. R., *Introduction to Modern Optics*. New York: Holt, Rinehart and Winston, Inc., 1968.

Freund, J. E. and Walpole, R. E., *Mathematical Statistics*, Third Edition. Englewood Cliffs, New Jersey: Prentice-Hall, Inc., 1980.

Halliday, D. and Resnick, R., *Fundamentals of Physics*, Second Edition, Extended Version. New York: John Wiley & Sons, Inc., 1981.

Harris, F. J., "On the Use of Windows for Harmonic Analysis with the Discrete Fourier Transform", *Proceedings of the IEEE*, Vol. 66, No. 1, January 1978, pp. 51-83.

Jakes, W. C., *Microwave Mobile Communications*, New York: John Wiley & Sons, Inc., 1974.

Molkdar, D., "Review on Radio Propagation into and within Buildings", *IEE Proceedings*, Vol. 138, No. 1, February 1991, pp. 61-73.

Morrison, G. D., *A Frequency Domain Measurement System for Indoor Ultrahigh Frequency Radio Propagation Studies*. Calgary, Alberta: Department of Electrical and Computer Engineering, 1991.

Oppenheim, A. V. and Schafer, R. W., *Digital Signal Processing*. Englewood Cliffs, New Jersey: Prentice-Hall, Inc., 1975.

Pahlavan, K. and Howard, S. J., "Frequency Domain Measurements of Indoor Radio Channels", *Electronic Letters*, Vol. 25, No. 24, November 23, 1989, pp. 1645-1647.

Press, W. H., Flannery, B. P., Teukolsky, S. A., and Vetterling, W. T., *Numerical Recipes in C: The Art of Scientific Computing*. Cambridge: Cambridge University Press, 1988.

Proakis, J. G., *Digital Communications*, Second Edition. New York: McGraw-Hill, Inc., 1989.

Rappaport, T. S., "Characterization of UHF Multipath Radio Channels in Factory Buildings", *IEEE Transactions on Antennas and Propagation*, Vol. 37, No. 8, August 1989, pp. 1058-1069.

Robinson, E. A. and Treitel, S., *Geophysical Signal Analysis.* Englewood Cliffs, New Jersey: Prentice-Hall, Inc., 1980.

Saleh, A. A. M. and Valenzuela, R. A., "A Statistical Model for Indoor Multipath Propagation", *IEEE Journal on Selected Areas in Communications*, Vol. 5, No. 2, February 1987, pp. 128-137.

Zaghloul, H., Fattouche, M., Morrison, G., and Tholl, D., "Comparison of Indoor Propagation Channel Characteristics at Different Frequencies", *Electronic Letters*, Vol. 27, No. 22, October 24, 1991, pp. 2077-2079.

Zaghloul, H., Morrison, G., Tholl, D., Davies, R. J., and Kazeminejad, S., "Frequency Response Measurements of the Indoor Channel", *Proceedings of Antem '90*, August 15-17, 1990, pp. 267-272.